Air Quality and Comfort Constrained Energy Efficient Operation of Multi-Zone Buildings

S. Naqvi[†], K. Kar[*], S. Bhattacharya[†], V. Chandan[‡], S. Mishra[*] and T. Salsbury[†]

[*]Rensselaer Polytechnic Institute, Troy, NY, USA, [†]Pacific Northwest National Laboratory, Richland, WA, USA, [‡] CrossnoKaye, Santa Barbara, CA, USA.

{kark, mishrs2}@rpi.edu[*], {ahsan.raza, saptarshi.bhattacharya, timothy.salsbury}@pnnl.gov[†], vikas@crossnokaye.com [‡]

Abstract

Maintaining indoor air quality (IAQ) through effective ventilation is essential for the well-being and productivity of building occupants. Control strategies aimed at improving the efficiency of heating, ventilation and air conditioning (HVAC) systems must jointly determine ventilation and heating and cooling processes. In this paper, we study the problem of minimizing the energy consumption of the HVAC system in a multi-zone building, while meeting thermal comfort and IAQ requirements. We first perform a steady state analysis of the zonal carbon dioxide (CO_2) concentration and the temperature dynamics. The resulting expressions are convex in the zonal mass flow rates and zonal temperatures. Guided by the steady state solutions for meeting the thermal comfort constraints, we develop two control policies for improving the energy efficiency of building HVAC systems while jointly satisfying indoor temperature and IAQ constraints. We compare the performance of our proposed approaches with those of multiple baseline approaches which implement separate regimes for controlling zonal temperature and IAQ for a typical work-day in a multi-zone campus building. We have evaluated the performance of our proposed approaches under varying levels of flexibility in zonal temperatures. We have shown that zonal temperature flexibility can result in energy savings up to 32% (for the same control strategies) as compared to the case where no such flexibility is permitted. Our proposed approaches were seen to offer potential savings of nearly 29% compared to the baseline.

Keywords– Multi-zone buildings, HVAC systems, indoor air quality, energy efficiency, thermal discomfort

S. Naqvi will serve as the corresponding author for this submission. Cell : +12054528762. Postal address: Apt. 04-12, 400 McChesney Ave. Ext., Troy, NY, USA, 12180.

NOMENCLATURE

Greek symbols

$\beta[k]$ Air handling unit (AHU) damper position at time instance k

Δ_j Temperature set-point (in °C) for zone j

δ_j Maximum permitted temperature flexibility about the temperature set-point in zone j

η Efficiency of the heating/cooling coil

μ Duration of each discrete time instance (in s)

Φ Total energy (in J) consumed by the heating/cooling coil

ϕ Cycling period (in s) for baseline ventilation control

ψ Pre-tuned gain for PI controller

ρ Density (in g/m^3) of air

σ CO_2 generation rate (in L/s) per person

ζ Indoor air quality violation metric

Number sets

$\mathcal{J}$ Set of all zones in a building

Other symbols

C_j Thermal capacitance of zone j (in J/°C)

c_p Specific heat capacity of air (in J/g/°C)

j Index of a zone

K Total number of discrete time instances

k Index for a discrete time instance

$\dot{m}_j[k]$ Instantaneous mass flow rate (in g/s) of air into zone j

$\dot{m}_j^{SS}[k]$ Steady state zonal air mass flow rates (in g/s) at time k

$\bar{m}$ Maximum permitted zonal mass flow rate (in g/s) of air

$O_j[k]$ Carbon dioxide (CO_2) concentration (in ppm) in zone j at time instance k

$O_{\text{mix}}[k]$ CO_2 concentration (in ppm) in the mixed air at time instance k

$O_{\text{out}}[k]$ CO_2 concentration (in ppm) in the ambient air at time instance k

$O_{j,\text{max}}$ Maximum permitted zonal CO_2 concentration (in ppm)

$O_j^{SS}[k]$ Steady state zonal CO_2 concentration (in ppm) at time instance k

$P[k]$ Power consumed (in W) by the heating/cooling coil at time instance k

R_j^o Thermal resistance (in °C/W) of the wall connecting zone j to the ambient

$T_\infty[k]$ Ambient temperature (in °C) at time instance k

$T_j[k]$ Temperature (in °C) of zone j at time instance k

T_S Constant temperature (in °C) of the air at the supply fan

$T_j^{\text{SS}}[k]$ Temperature (in °C) of zone j at steady state at time instance k

t Continuous time instance

V_j Volume (in m^3) of zone j

$Z_j[k]$ Occupancy in zone j at time instance k

1. INTRODUCTION

Heating, ventilation and air conditioning (HVAC) systems accounted for approximately 30% of the total energy consumed by the commercial building sector in the United States in 2017 [1]. In addition to meeting indoor heating/cooling demand, buildings must also meet indoor air quality (IAQ) standards, which impacts the building's power consumption profile. Building practitioners often participate in demand response (DR) to avoid high energy prices due to high demand in the grid. In this paper, we present an integrated approach for thermal and IAQ management in buildings that may or may not allow zonal temperature flexibility. We define *zonal temperature flexibility* as the practice of permitting indoor temperatures to vary within a given range about the set-point.

IAQ refers to the air quality within buildings and has a direct impact on the occupants' wellness and productivity [2], [3]. Given the emphasis on insulation and airtight construction for modern buildings, there is a need for implementing mechanical ventilation to draw in sufficient outdoor air into buildings [4] to ensure compliance with IAQ standards.

1.1 Literature Review

Research in the area of building HVAC control has mostly focused on ensuring the occupants' thermal comfort [5], [6]. However, there has been a growing interest in the field of IAQ management for HVAC systems. One of the primary aspects studied in the domain of building IAQ management involves the characterization of pollutant dynamics in an indoor space. This requires estimating the effects of the pollutant concentration in the ambient as well as those due to internal factors, such as zonal occupancy, on the instantaneous IAQ. Most prior work in this domain has used carbon dioxide (CO_2) concentration as an indicator for IAQ. Related work [7]–[9] has used machine learning (ML) as a tool for establishing the mapping between

instantaneous IAQ and multiple external and internal factors. For instance, the authors in [7] used ML to predict indoor CO_2 levels using inputs such as ambient temperature, relative humidity and dew points. The paper then proposed a control approach which used the CO_2 prediction mechanism to efficiently modulate the ventilation rate in a building. In contrast to [7]–[9] which used black box models for characterizing IAQ dynamics over time, we use a physics-based model to capture the temporal evolution of IAQ.

Past work in the field of IAQ management has studied multiple approaches for developing efficient ventilation mechanisms for indoor spaces. In this context, the authors in [8] developed a deep learning-based efficient ventilation optimization system for subway systems. Specifically, it used neural networks to predict day-ahead outdoor air quality conditions, while using particulate matter as a metric for air quality. It then went on to use dynamic programming to minimize the weighted sum of the particulate matter concentration and the energy consumption over a time horizon. Furthermore, in [9], the authors used historical CO_2 concentration levels and the corresponding supply fan speeds to predict the CO_2 concentration in the current time step in the indoor space. Aided by an indoor occupant number predictor, the authors developed a control framework for modifying ventilation rates in an anticipatory manner.

In addition to developing rule-based approaches for meeting IAQ standards in buildings, researchers have also used optimal control to meet the objectives of the building operator while satisfying IAQ requirements. For instance, [10] considered the compromise between IAQ management and energy consumption minimization. It proposed a distributed approach for IAQ management whereby individual control agents in each zone employed a model to predict the steady state CO_2 concentration. Subsequently, this model was used in the agents' objective function for determining the optimum ventilation air volume. A central controller then used these solutions to determine the ventilation air volumes to individual zones that minimize the total energy consumption. Similarly, in [11], the authors developed a particle swarm optimization-based approach to determine the optimal ventilation rate based on occupancy, outdoor air quality and the building volume. In [12], the authors used CO_2 as a metric for IAQ and used a genetic algorithm-based optimization for demand controlled ventilation to determine the upper and lower limits for indoor pollutant concentration for achieving desired IAQ levels while minimizing energy consumption and reducing the number of on-off cycles for the ventilation. Unlike our work, [12] only considered a single zone and stopped short of investigating how individual zones with different occupancy levels could affect the performance of the proposed approach.

The authors in [13] and [14] used reinforcement learning to meet zonal temperature and IAQ comfort requirements. In [13], the authors determined adaptive control decisions based on the current observations without requiring any prediction of system uncertainties. The paper used the instantaneous CO_2 concentration as the indicator for IAQ. The control approach used reinforcement learning to minimize the total system cost which was given by the sum of the energy cost, the cumulative violation of the IAQ constraints and the total thermal discomfort experienced by the occupants. Similarly, [14] used deep reinforcement learning to maintain thermal comfort and IAQ within permitted bounds, while minimizing energy consumption.

It is worth noting that of the papers [7]–[14], only [13] and [14] considered joint control for zonal temperatures and air quality. Furthermore, the aforementioned papers considered scenarios where ventilation was implemented at a zonal level. However, in several buildings, ventilation is controlled centrally and a single AHU damper needs to be controlled to maintain IAQ standards in multiple zones. Therefore, these papers stop short of considering the inter-dependency of zonal IAQ in a multi-zone building. Moreover, the use of data-driven control in [13], [14] meant that the authors did not address the non-convexities that arise in the control framework which simultaneously satisfies IAQ and temperature constraints.

While most prior work in the domain of comfort management in buildings has considered thermal and IAQ management separately, there is a need to develop a holistic approach for concurrently managing IAQ and indoor temperatures optimally. However, such a framework has been seen to be non-convex and difficult to optimize exactly. Due to this limitation, the authors in [15] developed an algorithm using Lyapunov optimization techniques to determine a feasible solution to an optimization framework that aimed to minimize energy costs from HVAC while meeting thermal comfort and IAQ requirements. As a step further, [16] formulated a bi-layer approach for integrated thermal and IAQ control. It was noted that while this methodology resulted in a sub-optimality of 4% with respect to the benchmark, it significantly reduced the execution time for solving the optimization problem for minimizing the power consumed by the HVAC system. Unlike [15] and [16], we study the integrated thermal and IAQ control problem under the presence and absence of zonal temperature flexibility. We show that for a building which permits zonal temperature flexibility, at steady state, the framework for minimizing the energy consumption in HVAC systems can be cast as a convex optimization problem when the zonal temperatures are taken to be the control variables. We also show that in the absence of zonal temperature flexibility, despite a bi-linear model structure, the framework decomposes into

two separate convex problems – one for determining the zonal air mass flow rates for thermal management and the other for determining the AHU damper positions for IAQ management. Finally, we have analysed the effect of different values of the permitted IAQ levels on zonal temperature and occupant comfort levels.

1.2 Open Challenges and Summary of Contributions

As previously stated, past work in the area of integrated IAQ and temperature management [15], [16] noted that the optimization problem considering system dynamics is hard to solve. Specifically, [15] developed a heuristic approach to jointly manage IAQ and zonal temperatures, which would generally not result in an optimum solution even under slow system dynamics. Similarly, the authors in [16] did not offer any guarantees regarding the optimality of the solution obtained from the control strategy proposed therein. In contrast, through this work, we hope to show that the joint IAQ and temperature management problem can be solved optimally at steady state or when the variations in the zonal occupancy patterns and the ambient temperature are slow compared to the heat and air flow dynamics in a building. Furthermore, while past papers have developed strategies for integrated IAQ and temperature management, they have stopped short of quantitatively justifying why it is desirable to jointly manage these indoor climate indicators. Finally, there is a need to develop a control strategy for jointly managing IAQ and zonal temperatures which is not only energy efficient but can also ensure the longevity of the building ventilation apparatus by reducing equipment wear-and-tear. In this context, while [12] developed a control strategy for enhancing the durability of the ventilation equipment, its scope was limited to only IAQ management in buildings. Our work aims to address these knowledge gaps in the state-of-the-art.

In this paper, we develop and evaluate control frameworks for energy efficient indoor climate control in a multi-zone building which minimize the energy consumption of the cooling coil in a variable air volume (VAV) HVAC system subject to thermal and IAQ constraints, while taking the CO_2 concentration in individual units as a metric for measuring IAQ. Specifically, we derive steady state expressions for the zonal mass flow rates and CO_2 concentrations as well as the power consumption of operating the cooling coil of the HVAC system. We show that these expressions are convex in the control variables for our framework. Utilizing the convex nature of this framework, we develop two multi-stage control policies for minimizing the energy consumption subject to zonal temperature and IAQ constraints under low complexity. The

resulting vectors of mass flow rates and zonal temperatures are then used to determine the control signals to the AHU damper for meeting the desired IAQ levels in the building. We then proceed to compare the performance of our approaches under varying zonal temperature flexibility with baselines that perform temperature and IAQ management operations independently of each other.

1.3 Specific Contributions and Technical Novelty

In the context of joint temperature and IAQ management in multi-unit buildings, our contributions to the state-of-the-art are multi-faceted.

Firstly, we provide a detailed convexity analysis of the mathematical expressions for the zonal temperatures and IAQ at steady state. We subsequently show that our proposed energy minimization framework is convex in the control variables at the steady state. We utilize the steady state analysis to obtain insights into the structure of the optimization problem and solve it in low complexity. To the best of the authors' knowledge, this work is the first in the domain of joint temperature and IAQ which provides such an analysis.

Secondly, we use the aforementioned analysis to develop two separate approaches for joint temperature and IAQ management for varying levels of zonal temperature flexibility permitted by the building operator in a multi-unit building. We compare the performances of our proposed control strategies with multiple benchmark approaches, which include current practices in IAQ management. Our study shows that our proposed approaches can achieve energy savings of up to nearly 29% as compared to the baseline strategies.

Thirdly, we evaluate the performance of the proposed joint temperature and IAQ management strategies under two dynamic temperature control strategies, i.e., proportional-integral (PI) control and hysteretic control (HC). Using the numerical results obtained from our simulation studies, we show that our proposed approaches can serve separate objectives for the building operator, such as enhancing system energy efficiency and preserving the durability of the building ventilation equipment.

Finally, using the performance of the baseline approaches, we quantitatively show why it is necessary for any control strategy aiming to improve building energy efficiency and occupant comfort to jointly manage zonal temperature and IAQ. This is especially true when the building operator participates in DR programs that introduce zonal temperature flexibility. In fact, we observe that the control strategy with the lowest energy consumption of all the approaches studied herein does not necessarily result in zonal temperatures settling at the upper limit of the

thermal dead-band. We further observe that modulating zonal temperature set-points within the permitted limits while implementing ventilation control is essential for maintaining IAQ.

The rest of this paper is organized as follows: Section 2 offers details on the system model and casts our proposed approach as a minimization problem. Section 3 provides a mathematical analysis and an exposition of our proposed control strategies for jointly handling zonal temperature and ventilation levels. Section 4 presents a discussion on the simulation results. Finally, Section 5 presents the conclusions of this paper.

2. System Model and Problem Formulation

We study an HVAC system similar to the one presented in [15]. Fig. 1 shows the schematic of the HVAC system considered in this work. Here, we consider a set $\mathcal{J}$ of zones in a building, with element j. Each unit has a temperature set-point, $\Delta_j, \forall j \in \mathcal{J}$. This system consists of an AHU for the entire building and a set of VAV boxes in each room. The AHU includes a damper, a cooling/heating coil and a fan. The damper helps mix the fresh air from outside with the air returning from each unit, while maintaining the required IAQ levels. The cooling/heating coils are used to bring the mixed air temperature to the desired levels. Finally, the fan delivers the mixed air to the VAV boxes in individual units. While the analysis that follows can be extended to apply for heating demand in buildings, here we primarily focus on the building cooling scenario.

2.1 The Thermodynamic Model

Taking $T_j(t)$ as the instantaneous temperature in unit j, R_j^o as the thermal resistance of the wall connecting unit j with the ambient, $T_\infty(t)$ as the ambient temperature at time t, C_j as the thermal capacitance of unit j, $\dot{m}_j(t)$ as the mass flow rate of air into unit j at time t, c_p as the specific heat capacity of air and T_S as the constant temperature of the air at the supply fan, the thermal dynamics in unit j are given by,

$$C_j \frac{dT_j(t)}{dt} = \frac{T_\infty(t) - T_j(t)}{R_j^o} + c_p \dot{m}_j(t)(T_S - T_j(t)). \tag{1}$$

In this work, we assume that the units are not thermally coupled with each other. The dynamics in (1) can be discretized for time instance k with duration μ as,

$$T_j[k+1] = \Big(1 - \frac{\mu}{R_j^o C_j}\Big) T_j[k] + \frac{\mu c_p}{C_j} \dot{m}_j[k](T_S - T_j[k]) + \frac{\mu}{R_j^o C_j} T_\infty[k]. \tag{2}$$

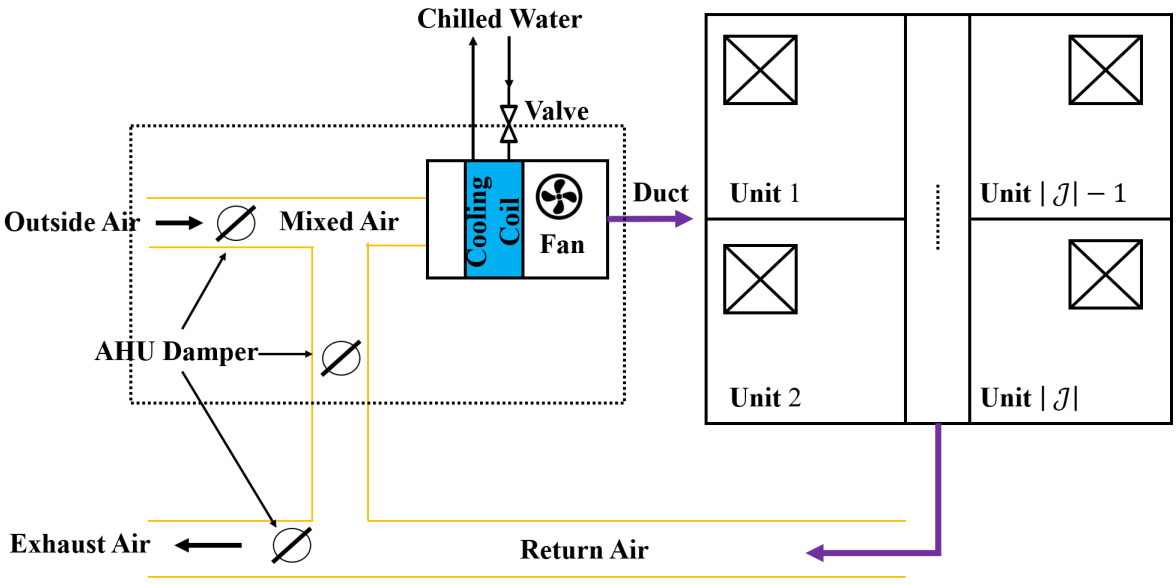

Fig. 1: Schematic of the overall HVAC system in our multi-unit building model.

2.2 The IAQ Model

In this work, we use the instantaneous zonal CO_2 concentration, measured in ppm, $O_j(t)$, as a metric for IAQ. The dynamics of CO_2 concentration in unit j are given by [17],

$$V_j \frac{dO_j(t)}{dt} = \frac{\dot{m}_j(t)}{\rho}(O_{\text{mix}}(t) - O_j(t)) + Z_j(t)\sigma, \tag{3}$$

where V_j is the volume of unit j in m^3, ρ is the air density in g/m^3, $Z_j(t)$ is the instantaneous occupancy of unit j and σ is the CO_2 generation rate per person in L/s. $O_{\text{mix}}(t)$ is the instantaneous mixed air CO_2 concentration, given by,

$$O_{\text{mix}}(t) = [1 - \beta(t)]O_{\text{out}}(t) + \beta(t)\frac{\sum_{j\in\mathcal{J}} O_j(t)\dot{m}_j(t)}{\sum_{j\in\mathcal{J}} \dot{m}_j(t)}, \tag{4}$$

where $\beta(t)$ is the position of the AHU damper at time t such that $0 \leq \beta(t) \leq 1$. When $\beta(t) = 0$, the AHU damper is said to be 'maximally open' while allowing the maximum possible amount of fresh air from the ambient to enter the system. Conversely, when $\beta(t) = 1$, the AHU damper is said to be 'maximally closed' thereby permitting only the air recycled from the individual zones to be circulated within the building. It is noteworthy that, as stated in [18], the damper may operate with quick opening (concave), linear or equal percentage (convex) characteristics. In our

work, we assume that the AHU damper operates with linear characteristics, i.e., the percentage opening of the AHU damper is directly proportional to the air flow rate through it. In view of this linear behavior, our work uses the $\beta[\cdot]$ variable as being representative of the physical position of the AHU damper. However, if the damper was taken to have either quick opening or equal percentage characteristics, the AHU damper position could be determined by transforming $\beta[\cdot]$ using a functional mapping.

The dynamics in (3) can be discretized for time instance k with duration μ seconds as,

$$O_j[k+1] = \Big(1 - \frac{\dot{m}_j[k]\mu}{\rho V_j}\Big)O_j[k] + \frac{\dot{m}_j[k]\mu}{\rho V_j}O_{\text{mix}}[k] + \frac{Z_j[k]\mu\sigma}{V_j}, \text{ where,} \tag{5}$$

$$O_{\text{mix}}[k] = [1-\beta[k]]O_{\text{out}}[k] + \beta[k]\frac{\sum_{j\in\mathcal{J}} O_j[k]\dot{m}_j[k]}{\sum_{j\in\mathcal{J}}\dot{m}_j[k]}. \tag{6}$$

2.3 Optimization Framework

Determining the optimal positions of the AHU damper and zonal air mass flow rates for minimizing the total energy consumed by the cooling/heating coil of the HVAC system, involves solving an optimization problem with the objective,

$$\min_{\beta[k],\dot{m}_j[k],T_j[k],O_j[k]\forall j,k}.\Phi, \tag{7}$$

where $\Phi = \mu\sum_{k=1}^{K} P[k]$ is the total energy consumed by the cooling coil and $P[k]$ is given by [15],

$$P[k] = \sum_{j\in\mathcal{J}} \dot{m}_j[k]\frac{c_p}{\eta\text{COP}}(\beta[k]T_j[k] + (1-\beta[k])T_\infty[k] - T_S).$$

Here, η is the efficiency of the cooling coil and COP is the coefficient of performance of the chiller. The objective (7) is optimized subject to,

$$(\text{C}_1) \quad (2),$$

$$(\text{C}_2) \quad (5),$$

$$(\text{C}_3) \quad 0 \le \dot{m}_j[k] \le \bar{m},\ \forall j,k,$$

$$(\text{C}_4) \quad -\delta_j \le T_j[k] - \Delta_j \le \delta_j,\ \forall j,k,$$

$$(\text{C}_5) \quad O_j[k] \le O_{j,\max}\ ,\forall j,k,$$

$$(\text{C}_6) \quad 0 \le \beta[k] \le 1,\ \forall k,$$

where $\bar{m}$ and δ_j are constants. In the formulation above, (C_1) and (C_2) establish the dynamics of zonal temperature and CO_2 concentration, constraint (C_3) imposes the upper and lower limits on the mass flow rate of air into unit j at time k, (C_4) allows zonal temperature to vary within a prescribed range about the temperature set-point, (C_5) imposes an upper limit on the instantaneous zonal CO_2 concentration and (C_6) imposes limits on the AHU damper position. It is noteworthy here that (C_6) in our optimization framework can be re-written as, $\beta_{\text{min}} \leq \beta[k] \leq \beta_{\text{max}}$, where β_{min} and β_{max} are constants representing lower and upper thresholds of $\beta[\cdot]$ to account for building codes which may impose restrictions on the minimum and maximum influx of ambient air into the building. Our solution extends easily to accommodate this change.

It can be observed that the expression for the CO_2 concentration in the mixed air in (6) introduces bi-linear terms into the optimization framework, causing it to become non-convex and hard to solve. In the subsequent section, we derive expressions for the zonal temperatures and CO_2 concentration levels at steady state and show that they are convex in the control variables. We then develop control strategies for minimizing (7) subject to thermal and IAQ constraints for given AHU damper positions.

3. Analysis and Control Algorithms

Observing the constraints of the optimization framework presented in the previous section leads us to consider two distinct operational cases from the standpoint of indoor temperature management. The first case represents the situation where the building operator does not permit flexibility in zonal temperatures and requires strict adherence to the set-point, Δ_j. Hence, this case takes $\delta_j = 0, \forall j$. As will be seen subsequently, this case significantly simplifies the solution to the proposed optimization framework. The second case takes $\delta_j > 0, \forall j$ and hence permits some flexibility in the zonal temperatures about Δ_j. In the sub-sections that follow, we use the steady state analysis for the zonal temperatures and CO_2 concentration to solve the energy consumption minimization problem given by (7) and constraints (C_1)-(C_6) in a computationally tractable manner. Henceforth, steady state zonal temperatures and CO_2 concentration will be denoted by $T_j^{SS}[\cdot]$ and $O_j^{SS}[\cdot]$, respectively.

We adopt a modular approach to achieve tractability in the optimization framework in (7). The first module determines the optimum values of $\dot{m}_j^{SS}[\cdot]$, the zonal air mass flow rates at steady state, and $T_j^{SS}[\cdot]$ that minimize the cooling coil energy consumption for satisfying the thermal comfort constraints for all units. The second module determines the AHU damper positions such

that the IAQ is maintained at all times for all units. Finally, the third module uses PI control or HC to drive the instantaneous zonal temperatures, $T_j[k]$, to $T_j^{SS*}[k]$.

In this section, we develop two control strategies for jointly managing indoor temperature and IAQ for both $\delta_j = 0$ and $\delta_j > 0$. The first strategy determines $T_j^{SS*}[\cdot]$, following which it uses PI control or HC to modulate the zonal air mass flow rates so that the instantaneous zonal temperatures track $T_j^{SS*}[\cdot]$. In the event of the CO_2 concentration in any of the zones exceeding the prescribed limit, $O_{j,\max}$, this strategy sets $\beta[k] = 0$ which results in only the outside air being supplied to the zones, causing a drop in zonal CO_2 concentration values. At all other time instances $\beta[k]$ is approximately equal to 1, meaning that there is minimal mixing of air from the outside with the air being re-circulated to the individual zones. Due to this switching operation of the AHU damper, we call this strategy "jointly optimal temperature and air quality control with on-off ventilation" (JOTAC-OOV). The second strategy determines the control inputs to the AHU damper, $\dot{m}_j^{SS*}[\cdot]$ and $T_j^{SS*}[\cdot]$ that minimize the cooling coil energy consumption at the steady state for a prescribed control window. Once the duration of the control window elapses, the system parameters are updated and these values re-evaluated, until the end of the planning horizon is reached. The strategy then uses PI control or HC to drive the instantaneous zonal temperatures, $T_j[k]$, to $T_j^{SS*}[k]$. Unlike JOTAC-OOV, this strategy takes $\beta[k]$ to be a continuous variable lying in the operational range prescribed in (C_6). Therefore, we call this control strategy "jointly optimal temperature and air quality control with fractional rate ventilation" (JOTAC-FRV). We will now proceed to studying the two distinct operational cases, i.e., the absence and the presence of zonal temperature flexibility separately, which will then lay the groundwork for the exposition of our proposed control policies.

3.1 Without Zonal Temperature Flexibility

3.1.1 Steady State Analysis

At steady state and for discretized time instances, with $\frac{dO_j(t)}{dt} = 0$ and using (4),(3) becomes:

$$\dot{m}_j^{SS}[k]\{(1-\beta^{SS})O_{\text{out}}[k] + \beta^{SS}\frac{\sum_{j\in\mathcal{J}} O_j^{SS}[k]\dot{m}_j^{SS}[k]}{\sum_{j\in\mathcal{J}}\dot{m}_j^{SS}[k]} - O_j^{SS}[k]\} = -Z_j[k]\sigma\rho, \tag{8}$$

where β^{SS} is the AHU damper position at the steady state. Taking $\kappa_j[k] = Z_j[k]\sigma\rho$, (3) becomes,

$$\dot{m}_j^{SS}[k](O_{\text{mix}}[k] - O_j^{SS}[k]) = -\kappa_j[k]. \tag{9}$$

Summing over all elements in $\mathcal{J}$, we have,

$$\sum_{j\in\mathcal{J}} \dot{m}_j^{SS}[k](O_{\text{mix}}[k] - O_j^{SS}[k]) = -\Lambda[k], \tag{10}$$

where $\Lambda[k] = \sum_{j\in\mathcal{J}} \kappa_j[k]$. Expanding (10), we have,

$$-\Lambda[k] = \sum_{j\in\mathcal{J}} \dot{m}_j^{SS}[k]\Big\{(1-\beta^{SS})O_{\text{out}}[k] + \beta^{SS}\frac{\sum_{j\in\mathcal{J}} O_j^{SS}[k]\dot{m}_j^{SS}[k]}{\sum_{j\in\mathcal{J}} \dot{m}_j^{SS}[k]}\Big\} - \sum_{j\in\mathcal{J}} \dot{m}_j^{SS}[k]O_j^{SS}[k]. \tag{11}$$

Taking $\dot{M}[k] = \sum_{j\in\mathcal{J}} \dot{m}_j^{SS}[k]$, we can rewrite (11) as,

$$-\Lambda[k] = \dot{M}[k](1-\beta^{SS})O_{\text{out}}[k] + \beta^{SS}\sum_{j\in\mathcal{J}} O_j^{SS}[k]\dot{m}_j^{SS}[k] - \sum_{j\in\mathcal{J}} O_j^{SS}[k]\dot{m}_j^{SS}[k], \tag{12}$$

$$\sum_{j\in\mathcal{J}} O_j^{SS}[k]\dot{m}_j^{SS}[k] = \frac{\Lambda[k]}{1-\beta^{SS}} + \dot{M}O_{\text{out}}[k]. \tag{13}$$

Plugging (13) into (8) and simplifying, we get,

$$O_j^{SS}[k] = O_{\text{out}}[k] + \frac{\beta^{SS}\Lambda[k]}{\dot{M}[k](1-\beta^{SS})} + \frac{\kappa_j[k]}{\dot{m}_j^{SS}[k]}. \tag{14}$$

At steady state, with $\frac{dT_j(t)}{dt} = 0$, (1) becomes:

$$\frac{T_\infty[k] - T_j^{SS}[k]}{R_j^o} + c_p\dot{m}_j^{SS}[k](T_S - T_j^{SS}[k]) = 0,$$

$$T_j^{SS}[k] = \frac{T_\infty[k] - T_S}{1 + c_p\dot{m}_j^{SS}[k]R_j^o} + T_S. \tag{15}$$

Using (15) we can express the power consumed by the cooling coil at discrete time instances k by,

$$P[k] = \sum_{j\in\mathcal{J}} \frac{\dot{m}_j^{SS}[k]c_p}{\eta\text{COP}}\Big\{\frac{\beta^{SS}(T_\infty[k] - T_S)}{1 + \dot{m}_j^{SS}[k]c_pR_j^o} + (1-\beta^{SS})(T_\infty[k] - T_S)\Big\}. \tag{16}$$

Since $\frac{\beta^{SS}}{1-\beta^{SS}}$ in (14) is convex for $\beta^{SS} \in [0, 1)$ and (16) is linear in β^{SS}, hence (14) and (16) are convex in β^{SS}.

3.1.2 Control Algorithms

$\mathbf{JOTAC-OOV-Stage\,I}$:- The optimum mass flow rates, $\dot{m}_j^{SS*}[\cdot]$, $\forall j,k$ are determined directly from equation (15) by setting $T_j^{SS}[\cdot]$ to Δ_j.

$\mathbf{JOTAC-OOV-Stage\,II}$:- A PI controller or HC is used to determine the air mass flow rates to each zone to drive $T_j[k]$ to $T_j^{SS}[k]$. The PI controller considered in this work uses a pre-tuned gain, denoted by ψ. The HC for zonal temperature control sets $\dot{m}_j[k]=\bar{m}$ when $T_j[k]$ exceeds the desired temperature by a fixed value. Conversely, once $T_j[k]$ falls below the desired temperature by a prescribed value, $\dot{m}_j[k]$ is set to 0. The variant of JOTAC-OOV which uses PI control for controlling the instantaneous zonal temperature will henceforth be called JOTAC-OOV-PI, whereas the one which uses HC for this purpose will be termed JOTAC-OOV-HC. The variant which employs neither PI nor HC and instead relies on the steady state solutions $\dot{m}_j^{SS*}[\cdot]$ and $T_j^{SS}[\cdot]$, $\forall j,k$ will henceforth be called JOTAC-OOV-SS.

$\mathbf{JOTAC-OOV-Stage\,III}$:- This stage sets the AHU damper such that it allows only the air from inside the building to circulate in the units ($\beta[k]\approx 1$) when the CO_2 concentration in all the units is below $O_{j,\max}$. However, if the instantaneous CO_2 concentration level in any of the units reaches or exceeds $O_{j,\max}$, $\beta[k]$ is set to 0 to allow more outside air to be brought into the building to improve the IAQ. The AHU damper remains at this position until the greatest CO_2 concentration in the building units falls below $O_{j,\max}$.

$\mathbf{JOTAC-FRV-Stage\,I}$:- Here, the computation of $\dot{m}_j^{SS*}[\cdot],\forall j,k$ is identical to that of Stage I for JOTAC-OOV for $\delta_j=0$, except that it is re-evaluated for each update of the control window.

$\mathbf{JOTAC-FRV-Stage\,II}$:- For each computation of the control window, we solve the following minimization problem:

$$\min_{\beta^{SS}} \quad \mu\sum_{k=1}^{K} P[k] \;\; \text{s.t.} \;\; (14),(\mathrm{C}_5), \tag{17}$$

where $P[k]$ is given by (16). As shown in Section 3.1.1, the framework in (17) is convex in β^{SS}. The JOTAC-FRV approach sets the AHU damper position to β^{SS*}, the optimal solution for (21), obtained after each computation of the control window. If, however, the predicted IAQ from (5) using $m_j[k]=m_j^{SS}[k]\;\forall j,k$ is greater than $O_{\max}$, we iteratively reduce β^{SS*} by a small value, α, until the IAQ requirements are met.

$\mathbf{JOTAC-FRV-Stage\,III}$:- A PI controller or HC is used to determine the air mass flow rates to each zone to drive $T_j[k]$ to $T_j^{SS}[k]$. The variant of JOTAC-FRV which uses PI control for controlling the instantaneous zonal temperature will henceforth be called JOTAC-FRV-PI,

whereas the one which uses HC for this purpose will be termed JOTAC-FRV-HC. The variant which employs neither PI nor HC and instead relies on the steady state solutions $\dot{m}_j^{SS*}[\cdot]$ and $T_j[\cdot]$, $\forall j, k$ will henceforth be called JOTAC-FRV-SS.

3.2 With Zonal Temperature Flexibility

3.2.1 Steady State Analysis

The air mass flow rates, zonal CO_2 concentrations and power consumption at steady state can also be expressed in terms of $T_j^{SS}[\cdot]$. Rearranging the terms in (15), we get,

$$\begin{aligned}\dot{m}_j^{SS}[k] &= -\frac{(T_\infty[k]-T_S)/(R_j^o c_p T_S)}{1-\frac{T_j^{SS}[k]}{T_S}} - \frac{1}{R_j^o c_p} \\ &= -\frac{(T_\infty[k]-T_S)/(R_j^o c_p T_S)}{1-\frac{T_j^{SS}[k]}{T_S}} - \frac{1}{R_j^o c_p}. \end{aligned} \tag{18}$$

Plugging this expression for $\dot{m}_j^{SS}[k]$ in (14), we get,

$$\begin{aligned} O_j^{SS}[k] = O_{\text{out}}[k] &- \frac{\frac{\beta^{SS}\Lambda[k]c_p}{(1-\beta^{SS})}}{\left(\sum_{j\in\mathcal{J}}\frac{1}{R_j^o}\right)} \\ &\qquad \frac{}{\sum_{j\in\mathcal{J}}\frac{1}{T_j^{SS}[k]}} \\ &\qquad 1+\frac{T_\infty[k]-T_S}{T_S}\frac{R_j^o(1-\frac{T_j^{SS}[k]}{T_S})}{\sum_{j\in\mathcal{J}}\frac{1}{R_j^o}} \\ &- R_j^o\kappa_j[k]c_p + \frac{R_j^o\kappa_j[k]c_p(T_\infty[k]-T_S)/T_\infty[k]}{1-\frac{T_j^{SS}[k]}{T_\infty[k]}}. \end{aligned} \tag{19}$$

Finally, plugging (18) in (16), we get,

$$\begin{aligned} P[k] = \sum_{j\in\mathcal{J}} &\frac{\beta^{SS}(T_\infty[k]-T_S)}{\eta\text{COP}R_j^o T_S}\left(1-\frac{1}{1-\frac{T_j^{SS}[k]}{T_S}}\right) - \\ &\frac{\beta^{SS}}{R_j^o\eta\text{COP}}T_j^{SS}[k] - \frac{(T_\infty[k]-T_S)/(R_j^o c_p)}{1-\frac{T_j^{SS}[k]}{T_S}} - \\ &\frac{c_p(1-\beta^{SS})T_\infty[k]}{\eta\text{COP}}. \end{aligned} \tag{20}$$

The right hand side of (18) can be expressed as $-\frac{\gamma_1[k]}{1-\frac{T_j^{SS}[k]}{T_S}} - T_S$, where $\gamma_1[\cdot]$ and T_S are positive constants in the case where the building requires cooling. Since, $\frac{d^2\dot{m}_j[k]}{dT_j[k]^2} > 0$, hence the expression is convex in $T_j^{SS}[k]$. Furthermore, in (19), the dependencies of the second and fourth terms on $T_j^{SS}[k]$ are of the forms $-\frac{1}{1+\frac{1}{1-\frac{T_j^{SS}[k]}{T_S}}}$ and $\frac{1}{1-\frac{T_j^{SS}[k]}{T_\infty[k]}}$. As the cooling scenario is given by the inequalities, $T_\infty[k] > T_j^{SS}[k] > T_S$, hence these terms are convex in $T_j^{SS}[k]$. A similar

logic can be used for proving the convexity of (20) in $T_j[k]$. The analysis above can be readily extended to the heating scenario as well, where we have $T_\infty[k] < T_j^{SS}[k] < T_S$.

3.2.2 Control Algorithms

$\mathbf{JOTAC-OOV-Stage\,I}$:- Here, we solve the following optimization problem:

$$\min_{T_j^{SS}[k],\forall j,k} . \ \mu \sum_{k=1}^{K} P[k] \ \text{ s.t. } \ (18), (19), (\mathrm{C}_3), (\mathrm{C}_4), (\mathrm{C}_5), \tag{21}$$

where $P[k]$ is given by (20), while searching over the range $\beta^{SS} \in [0, 1)$. As shown in Section 3.2.1, the framework in (21) is convex in $T_j^{SS}[k]$. The value of $\bar{\beta}$ that results in the lowest total energy consumption in (21) is denoted by $\bar{\beta}^*$, the corresponding steady state zonal temperatures are denoted by $T_j^*[\cdot], \forall j, k$, and the corresponding steady state zonal mass flow rates are denoted by by $\dot{m}_j^*[\cdot], \forall j, k$.

$\mathbf{JOTAC-OOV-Stage\,II}$:- This stage is identical to Stage II for JOTAC-OOV when $\delta_j = 0$.

$\mathbf{JOTAC-OOV-Stage\,III}$:- This stage is identical to Stage III for JOTAC-OOV when $\delta_j = 0$.

$\mathbf{JOTAC-FRV-Stage\,I}$:- The computations here are similar to those in Stage I for JOTAC-OOV when $\delta_j > 0$ and are performed at every update of the control window.

$\mathbf{JOTAC-FRV-Stage\,II}$:- This stage adopts the β^{SS} (and the corresponding $T_j^{SS}[\cdot]$ and $\dot{m}_j^{SS}[\cdot]$) resulting in the lowest energy consumption while satisfying the IAQ constraints at the steady state (19) and the transient state (5) when $m_j[k] = m_j^{SS}[k] \ \forall j, k$.

$\mathbf{JOTAC-FRV-Stage\,III}$:- This stage is identical to Stage III of JOTAC-FRV when $\delta_j = 0$.

Fig. 2 summarizes the aforementioned JOTAC approaches presented in this work.

4. Numerical Study

In this section, we present simulation results for our proposed control algorithms at different times of the day in a multi-zone campus building equipped with a VAV HVAC system. All numerical results presented in this work have been obtained by running simulations in MATLAB. The AHU damper is assumed to change its positions from one extreme to the other instantaneously. For simulation purposes, we consider the campus building model to comprise of three zones, indexed as $\mathcal{J} = \{1, 2, 3\}$. Our simulations use $\mu = 60$s, $K = 60$, $O_{\text{out}}[k] = O_{\text{out}} = 415$ppm $\forall k$ [19] and $\rho = 1290$g/m^3. The minimization problem for the JOTAC-OOV approach (see Fig. 2a) is solved once every hour. Moreover, the control window for the JOTAC-FRV approach (see Fig. 2b) has a duration of 15 minutes, following which the steady state minimization problem is re-solved.

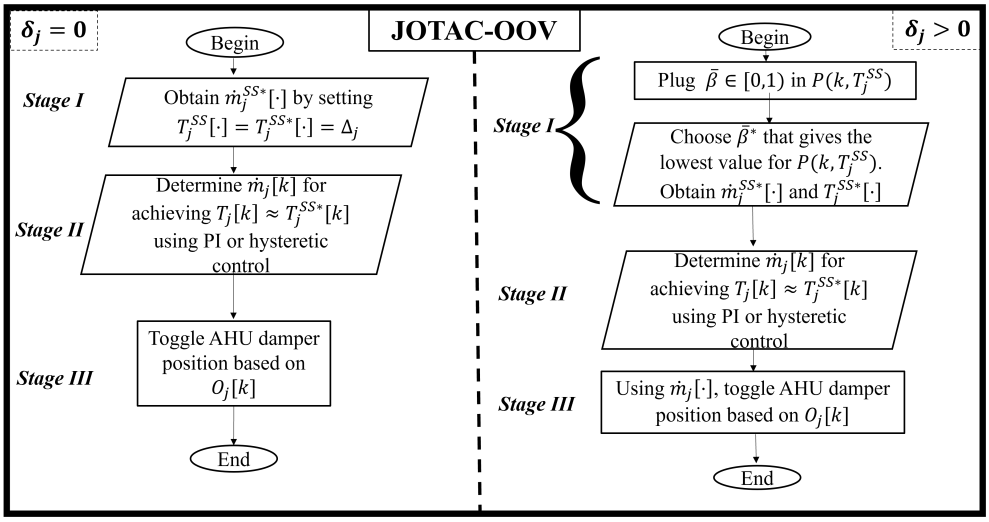

(a)

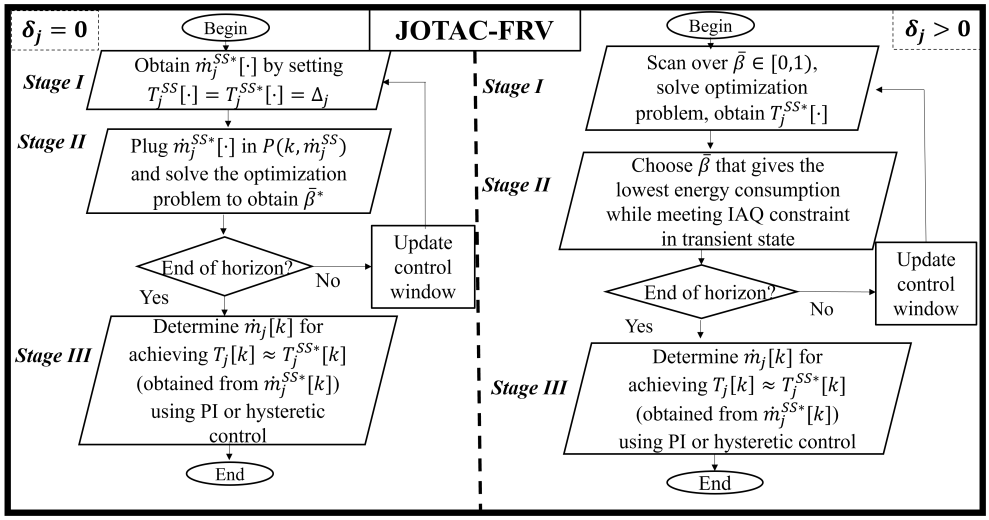

(b)

Fig. 2: Summary of control algorithms presented in this work; (a) JOTAC-OOV and (b) JOTAC-FRV.

In this work, we consider three values of $O_{j,\max} = O_{\max} \in \{500, 765, 1115\}$ppm to account for varying degrees of IAQ required to be maintained by the building operator while adhering to ASHRAE standards [20]. We take $O_j[0]$ in the lecture halls to be $0.999O_{\max}$, whereas that in the hallway to be $0.99O_{\max}$ in all cases. The temperature set-point in each zone, Δ_j, is taken to be 20°C. R_1^o, R_2^o and R_3^o are 0.0053°C/W, 0.0060°C/W and 0.0067°C/W [15], respectively. Furthermore, using the values in [15], we take $\bar{m} = 450$g/s, $\eta = 0.8879$, COP $= 5.9153$,

$c_p = 1.012$J/g/°C, $T_S = 12.8$°C and $\sigma = 0.0052$L/s. The PI controller used throughout the study uses $\psi = 200$. The hysteretic temperature controller considered in this work begins cooling when zonal temperatures exceed the set-point by 0.5°C, until the instantaneous zonal temperature falls to 0.5°C below the desired zonal temperature.

As stated previously, we consider a multi-zone campus building model for evaluating the performance of our proposed control strategies. Two of these zones are assumed to have a maximum occupancy comparable to that of a large lecture hall based on ANSI/ASHRAE Standard 62.1 2016 [21], whereas the third zone is significantly smaller and represents a hallway. For presentation purposes, we use indices $j = 1, 2$ to represent the lecture halls and index $j = 3$ to denote the hallway. In the results that follow, using the square footage guidelines for campus lecture halls from [22], we take $V_j = 1225\text{m}^3$ for $j \in \{1, 2\}$ and $V_3 = 480\text{m}^3$. The thermal capacitances for each zone are determined using $C_j = \rho \cdot c_p \cdot V_j$. In this work, we study the performance of our proposed control strategies for a typical work-day at campus, from 6 AM to 7 PM, while assuming that zonal occupancies are either accurately determined or are well-estimated. The occupancy levels in the lecture halls, as seen in Figs. 3a and 3b reflect the periods when classes are in session. During these sessions, students may temporarily leave the lecture halls which are reflected by a decrease in the number of occupants of these halls, as seen in Figs. 3a and 3b. Throughout this work, the hallway is taken to be a thoroughfare where individuals are not expected to spend a significant amount of time, allowing the building operator to implement a greater degree of temperature flexibility in this zone for saving energy costs. This observation allows us to study the performance of our control approaches when there are varying degrees of temperature flexibility within the same building. Since this work primarily aims to provide a comparative study of the JOTAC approaches presented earlier with some baseline approaches for varying zonal occupancy keeping all external variables to be constants, most of the results presented herein assume that $T_\infty[k] = 30$°C, $\forall k$. However, towards the end of this section, we include a set of results that considers diurnal temperature variation as well.

As previously stated, this numerical study also explores the effect of zonal temperature flexibility in the building on the performance of our proposed control policy. To this end, we study the case where the building operator requires strict adherence to temperature set-points at all times (i.e., $\delta_j = 0, \forall j$) as well as that where the operator permits the zonal temperatures to vary within a prescribed temperature range about the set-point (i.e., $\delta_j > 0, \forall j$). For the situation where $\delta_j > 0$, we consider two further scenarios: Scenario I and Scenario II. Scenario

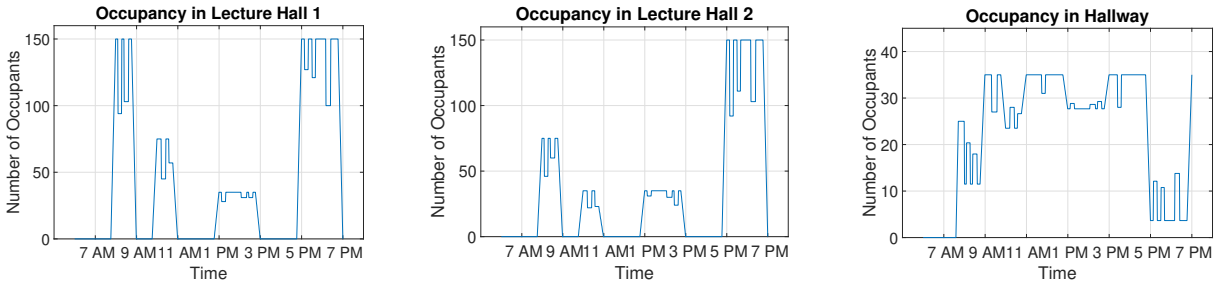

(a) (b) (c)

Fig. 3: Change in occupancy levels in (a) Lecture Hall 1; (b) Lecture Hall 2 and (c) the Hallway between 6 AM and 7 PM.

I sets $\delta_j = 1, \forall j$, whereas Scenario II implements a greater degree of temperature flexibility for cooling operations in the hallway using $\delta_3 = 10$, while keeping $\delta_j = 1$ for $j \in \{1, 2\}$. Through these special cases, we hope to determine if relaxing the thermal comfort requirements in certain zones within a building can help reduce the building's dependence on drawing outside air for IAQ management.

In this work, we compare the performance of the JOTAC strategies with separate baselines for when the building operator permits zonal temperature flexibility as well as when no such flexibility is available. Two further categories of the baseline approaches have been studied for comparison. The first category assumes perfect estimates for the instantaneous zonal occupancy and is therefore called the instantaneous occupancy-based (IO) approach. In contrast, the second category, which we call the design occupancy-based (DO) approach, determines HVAC controls for maintaining IAQ when all zones are maximally occupied. To ensure a fair comparison between our proposed strategies and the baselines, we have evaluated their performance using identical ambient and starting conditions, as well as thermal comfort and IAQ requirements, in each case.

4.1 Absence of Zonal Temperature Flexibility, $\delta_j = 0$, $\forall j$

4.1.1 Baselines

a) DO Baseline Using HC (B-DO-HC)

This baseline approach determines optimum steady state mass flow rates, $\dot{m}_j^{SS*}[\cdot], \forall j, k$ directly from equation (15) by setting $T_j^{SS}[\cdot]$ to Δ_j. It then determines the hourly AHU damper position

setting, $\beta[\cdot]$ required to keep the steady state CO_2 concentration in each zone to be less than or equal to $O_{\max}$ when the occupancy in each of the zones is at the design limit. Then, for a given cycling period of ϕ minutes, the AHU damper position is kept maximally open for $\phi \cdot (1 - \beta[k])$ minutes and maximally closed for the remainder of the period. This action is repeated for the rest of the hour until the value for the AHU damper position is determined for the subsequent hour and the process is repeated. The ventilation operations in this baseline technique is comparable to the intermittent ventilation approaches considered in [7], [12], [23].

b) DO Baseline Using PI (B-DO-PI):

This baseline is identical to B-DO-HC other than the use of a PI controller for thermal management in the building.

4.1.2 Results

Figs. 4a depicts the temporal evolution of CO_2 concentration in the building for the JOTAC-OOV-HC when $O_{\max} = 500$ppm. The figure shows how the JOTAC-OOV-HC policy generally ensures that the zonal CO_2 concentration in the entire building remains below $O_{\max}$ by alternating between the AHU damper being maximally open and maximally closed depending on the IAQ in each of the three zones studied here. However, two intervals, as demarcated in Fig. 4a, require particular attention. The first period, as shown in Fig. 4b, shows that around 8 AM, at time instance k_1, $O_1[k_1]$ continues to increase beyond $O_{\max}$, despite $\beta[k_1] = 0$. This could be attributed to the fact that the dynamic temperature control for this strategy is implemented using HC. This means that the air mass flow rate to each zone, $\dot{m}_j[k]$, only takes values in the set $\{0, \bar{m}\}$ depending on the instantaneous zonal temperature. As shown in Fig. 4b, $\dot{m}_1[k_1] = 0$ which means that, irrespective of the AHU damper position, Lecture Hall 1 does not receive the required air mass from the central VAV HVAC system to restore the IAQ to within permissible bounds. In contrast, at time instances k_2 and k_3, the mass flow rates to the Lecture Hall 2 and the hallway increase from 0 to $\bar{m}$ and, with $\beta[k] = 0$, in turn witness a sharp decline in the zonal CO_2 concentration subsequently. It is only at k_4 (where $k_4 > k_3 > k_2$) that the air mass flow rate to Lecture Hall 1 increases to $\bar{m}$, thereby allowing the influx of air from the ambient to the zone and, in the process, improving the IAQ until $O_1[k] < O_{\max}$ following which β is reset to 1.

The second interval of interest in this study is shown in Fig. 4c. Here, the AHU damper is maximally open at time instance k_5 as the CO_2 concentration in the hallway exceeds $O_{\max}$. Owing to the prevailing zonal temperature in Lecture Hall 1, the instantaneous air mass flow

rate to this zone at k_6 is $\bar{m}$, which channels air from the outside to Lecture Hall 1 and, in doing so, brings about a fall in the CO_2 concentration in that zone. The AHU damper remains maximally open during the interval between k_6 and k_7 causing a further decrease in $O_1[\cdot]$. At k_7, $\dot{m}_3 = \bar{m}$ which then reduces $O_3[k]$ to below $O_{\max}$, following which the AHU damper is closed. Beyond k_8, Lecture Hall 2 also experiences a gradual decrease in zonal CO_2 concentration. This observation can be attributed to the fact that the improved IAQ in Lecture Hall 1 and the hallway results in a decrease in the CO_2 concentration in the mixed air being supplied to each zone. With $\dot{m}_2[k_8] = \bar{m}$, Lecture Hall 2 benefits from the improved IAQ in the other two zones as it witnesses a decrease in its own zonal CO_2 concentration. The results in Fig. 4 should impress upon the reader the interdependence of the zonal temperature control and the indoor ventilation control loops.

Fig. 5 plots the temporal evolution of CO_2 concentration in the building for the JOTAC-FRV-HC approach when $\delta_j = 0, \forall j$. As the JOTAC-FRV approach takes $\beta[\cdot]$ to be a continues variable with values ranging between 0 and 1, it kept the AHU damper partially open to continually draw a limited quantity of air from the ambient, thereby ensuring that, in this case, the IAQ remained within permitted bounds.

Table I presents the energy consumed (in MJ) by our proposed JOTAC approaches, along with the energy consumed by the baseline approaches B-DO-HC and B-DO-PI. It may be seen that while the energy consumption for the JOTAC-OOV and JOTAC-FRV approaches are fairly close, these control strategies offer significant energy savings compared to the DO-based baselines in the absence of zonal temperature flexibility. Furthermore, it may be seen that there is a decreasing trend in the energy consumption for the JOTAC approaches for increasing value of $O_{\max}$. It is worth noting here that, as previously mentioned, the initial zonal IAQ in each case is taken to be close to the corresponding value of $O_{\max}$. Therefore, for increasing values of $O_{\max}$, the gradient between the instantaneous zonal and ambient CO_2 concentrations becomes progressively steeper. This, in turn, means that at greater values of $O_{\max}$, nominal modulations in the AHU damper position for brief periods can bring about significant improvements in zonal CO_2 concentrations. As the AHU damper is engaged less frequently under these conditions, thereby causing a reduction in the energy consumed by the cooling coil of VAV HVAC system. Fig. 6 quantifies the benefits of using the control policies presented herein as opposed to the baselines under consideration.

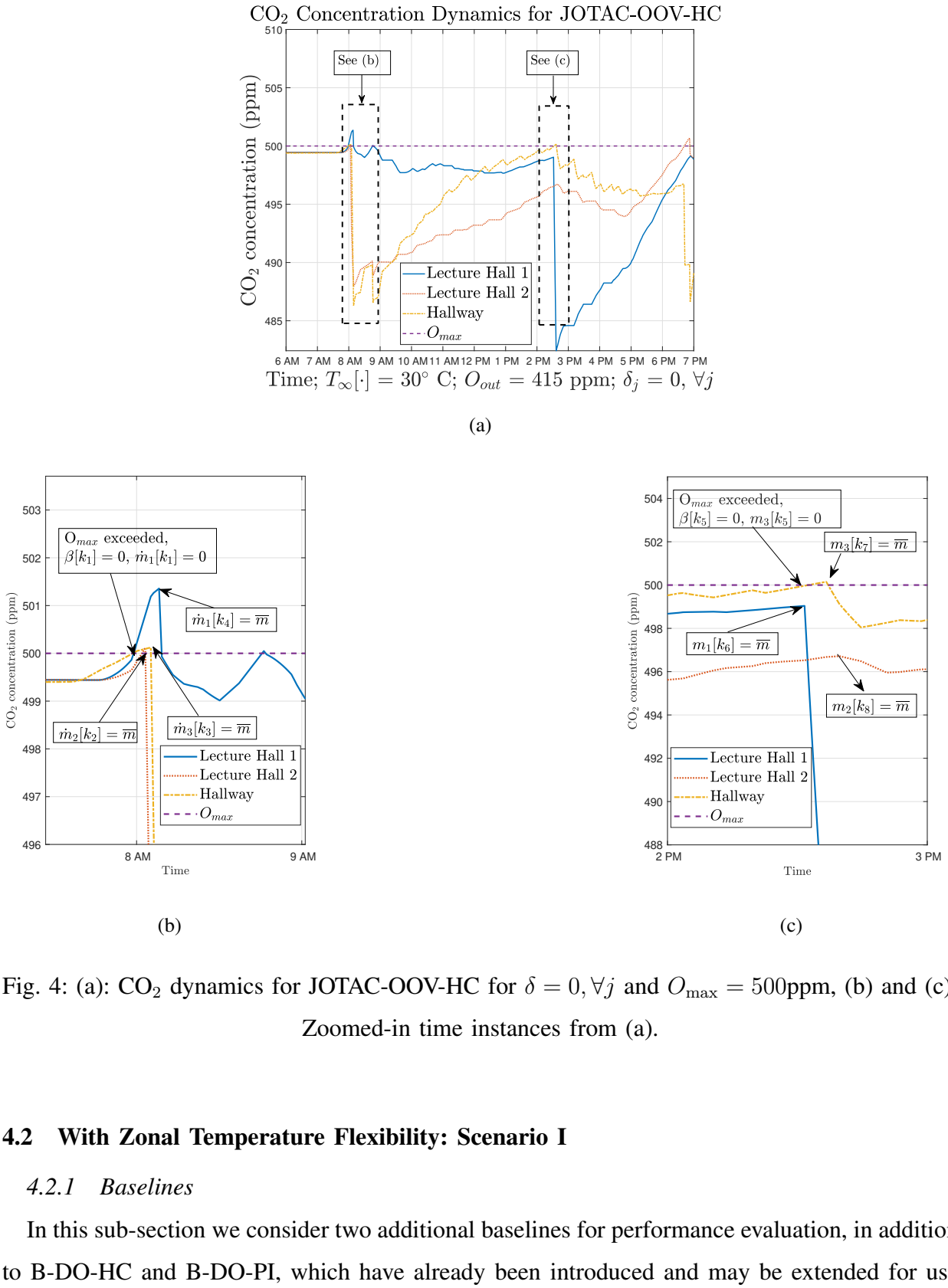

Fig. 4: (a): CO_2 dynamics for JOTAC-OOV-HC for $\delta = 0, \forall j$ and $O_{\max} = 500$ppm, (b) and (c): Zoomed-in time instances from (a).

4.2 With Zonal Temperature Flexibility: Scenario I

4.2.1 Baselines

In this sub-section we consider two additional baselines for performance evaluation, in addition to B-DO-HC and B-DO-PI, which have already been introduced and may be extended for use when $\delta_j > 0, \forall j$. Specifically, these baseline approaches maintain zonal temperatures at $\Delta_j + \delta_j$,

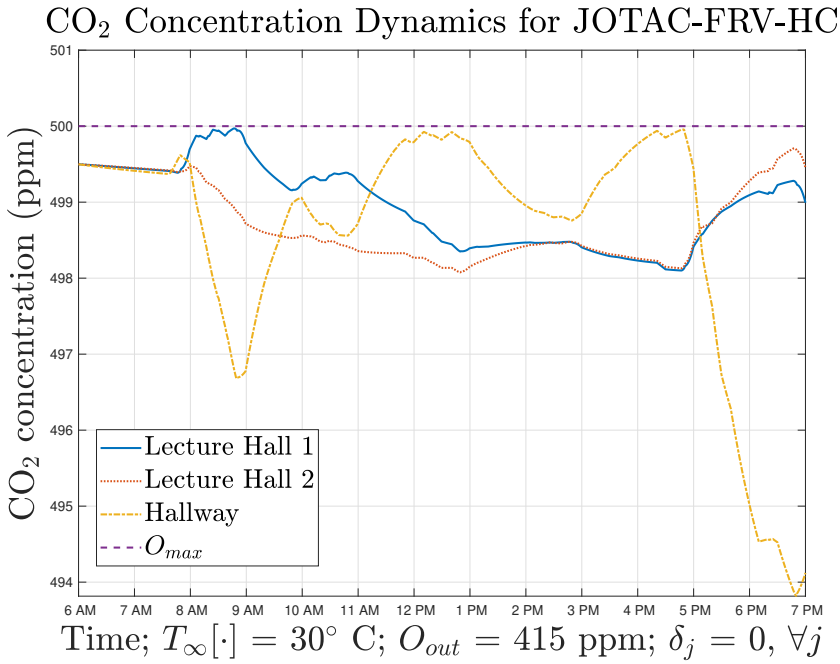

Fig. 5: CO_2 dynamics when $\delta_j = 0, \forall j$ and $O_{\max} = 500$ppm for the JOTAC-FRV-HC approach.

TABLE I: Energy consumption of the proposed JOTAC approaches (in MJ) as well as the DO-based baselines for $\delta_j = 0, \forall j$.

$O_{\max}$	**OOV-PI**	**FRV-PI**	**OOV-HC**	**FRV-HC**	**OOV-SS**	**FRV-SS**	**B-DO-HC**	**B-DO-PI**
500	41.8	45.0	42.5	45.3	41.7	46.2	57.7	57.7
765	41.1	44.7	41.5	45.0	41.0	45.1	57.7	57.7
1115	41.0	44.7	41.3	45.0	40.9	44.8	57.7	57.7

$\forall j$, using HC and PI control, respectively.

a) IO Baseline Using HC (B-IO-HC)

This approach assumes that the instantaneous zonal occupancy is well-estimated at all times. Additionally, it implements separate control mechanisms for zonal IAQ and temperature management. Specifically, it uses HC for maintaining zonal temperatures close to $\Delta_j + \delta_j$, $\forall j$, and an on-off control approach for IAQ management, similar to Stage II of JOTAC-OOV.

b) IO Baseline Using PI Control (B-IO-PI)

This baseline is identical to B-IO-HC other than the fact that it uses a PI controller for thermal management in the building.

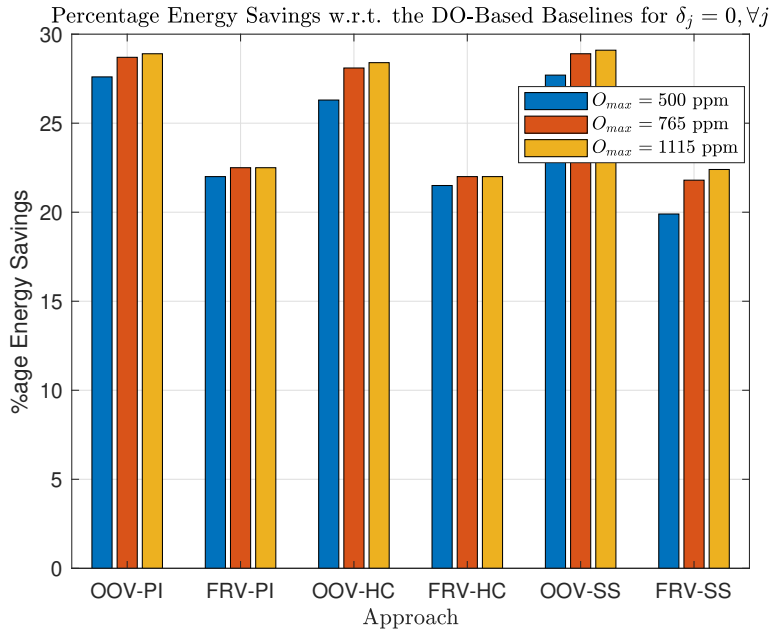

Fig. 6: Percentage (%) savings of the proposed JOTAC approaches w.r.t. the DO-based baselines for $\delta_j = 0, \forall j$.

It is noteworthy that unlike our proposed JOTAC approaches, the baselines reflect variants of the business-as-usual operations in buildings which completely decouple the temperature management and ventilation control operations in the building. Furthermore, it may be observed that as the IO baselines would have been identical to the corresponding JOTAC-OOV approaches for $\delta_j = 0, \forall j$, we did not include their evaluation results in Section 4.1.2. We will now present the performance of our proposed strategies compared to the aforementioned baselines, starting with the case where the building operator does not permit zonal temperature flexibility.

4.2.2 Results

Here, we will evaluate the performance of our proposed JOTAC strategies as opposed to the previously-defined baselines for the situation where the building operator permits a temperature flexibility of up to 1°C about Δ_j in each of the three zones. Table II presents the total energy consumed by the proposed control strategies and the baselines. Given the nature of the objective function in (7) as well as the baselines, all zonal temperatures were seen to settle at or close to 21°C It may be seen that the DO-based approaches, B-DO-HC and B-DO-PI, consume the greatest energy. As the JOTAC-FRV approaches determine the AHU damper position which minimizes energy consumption at the steady state, the resulting ventilation control proved to

TABLE II: Energy consumption of the proposed JOTAC approaches and the baselines (in MJ) for Scenario I.

$O_{\max}$	**OOV-PI**	**FRV-PI**	**OOV-HC**	**FRV-HC**	**OOV-SS**	**FRV-SS**	**B-DO-HC**	**B-DO-PI**	**B-IO-HC**	**B-IO-PI**
500	37.7	43.1	37.9	43.3	37.8	42.6	49.5	50.0	38.4	37.7
765	36.9	41.8	36.8	42.2	37.0	41.7	49.5	50.0	37.0	36.9
1115	36.8	41.8	36.7	42.1	36.9	41.7	49.5	50.0	36.7	36.8

be a conservative strategy for controlling the IAQ. This caused the variants of the JOTAC-FRV approach to consume more energy than B-IO-HC and B-IO-PI. Given the restricted zonal temperature flexibility, the steady state solutions for zonal temperatures determined by JOTAC-OOV-PI remained close to 21°C. As the baselines require zonal temperatures to necessarily settle at $\Delta_j + \delta_j$ and since the ventilation control is handled in an identical manner for B-IO-HC, B-IO-PI and JOTAC-OOV, hence JOTAC-OOV-PI was seen to have an energy consumption value which was approximately equal to that of B-IO-PI. Furthermore, it may be seen that the energy consumption for the JOTAC approaches as well as that for B-IO-HC and B-IO-PI, decreased for increasing values of $O_{\max}$. An explanation for this trend has already been provided in the discussion for the results for $\delta_j = 0, \forall j$.

Fig. 7 plots the instantaneous AHU damper position, $\beta[k]$, over the course of the simulation horizon for the JOTAC-OOV-SS and JOTAC-FRV-SS approaches for Scenario I when $O_{\max} = 500$ppm. It may be seen that the value of $\beta[k]$ undergoes several transitions from approximately 1 to 0 for JOTAC-OOV-SS in order to maintain IAQ in all the zones in the building. In contrast, the JOTAC-FRV-SS approach resulted in a much smoother trend for the values of $\beta[k]$. This observation can be attributed to the fact that the JOTAC-FRV-SS approach jointly determines the optimum combination of steady state zonal temperatures and the corresponding AHU damper position for minimizing the total energy consumed at the steady state (16). It was seen that as long as the steady state zonal temperatures were sufficiently modulated within the prescribed range of temperatures during each control window, some finer adjustments to the AHU damper position could be made to ensure that the IAQ standards were met at all times. Although Table II showed that the JOTAC-FRV-SS consumed greater energy than the JOTAC-OOV-SS approach, the smooth transitions in the AHU damper position implemented by the former can help enhance the durability of the building's ventilation apparatus, as explained in [12]. It was also seen that

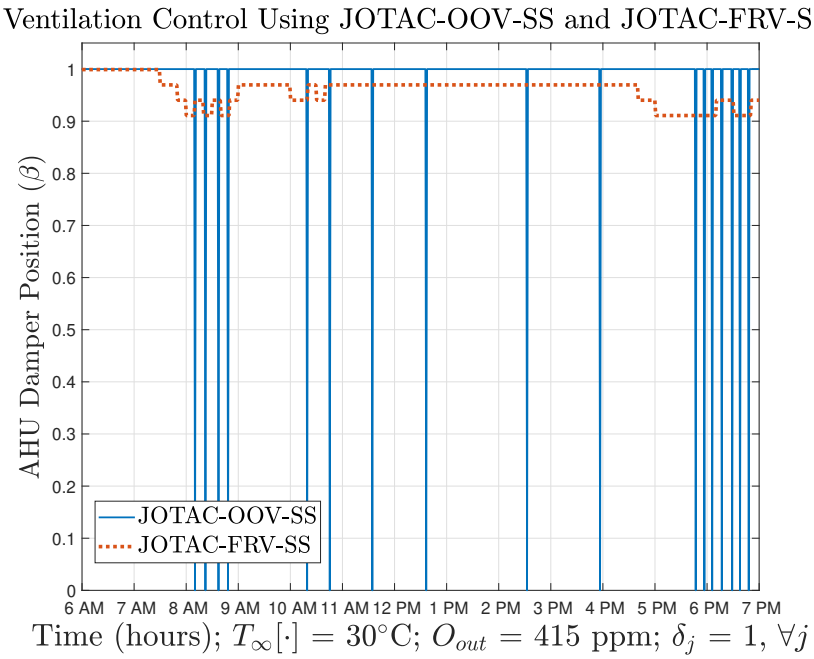

Fig. 7: Ventilation control for Scenario I when $O_{\max} = 500$ppm for the JOTAC-OOV-SS and JOTAC-FRV-SS strategies.

the mean normalized frequency (with respect to the sampling frequency) of the control signal to the AHU damper for JOTAC-OOV-SS was 2 orders greater than that for JOTAC-FRV-SS. This was due to the several transitions in AHU damper position from one extreme to the other as effected by JOTAC-OOV-SS. Specifically, the mean normalized frequencies for JOTAC-OOV-SS and JOTAC-FRV-SS were 0.0349 and 0.000333, respectively. The choice between the two JOTAC approaches is therefore dependent on the objectives and operational preferences of the building operator.

4.3 With Zonal Temperature Flexibility: Scenario II with Constant Ambient Temperatures

In this sub-section we present the results for the case when $\delta_3 = 10$, with the permitted temperature flexibility being $\pm 1°$C about Δ_j in the two lecture halls. The first phase of this study will provide a comparative analysis of the results for JOTAC-OOV and JOTAC-FRV approaches. We will then study the respective performances of our proposed control strategies with those of the baselines described in 4.2.1.

Fig. 8a plots the temporal evolution of zonal CO_2 concentration in the building for the JOTAC-OOV-HC approach, whereas Figs. 8b and 8c present the steady state and instantaneous zonal

temperatures for the JOTAC-OOV-HC and JOTAC-OOV-PI approaches, respectively. Finally, Figs. 8d, 8e, 8f, 8g, 8h, 8i show the temporal evolution of zonal CO_2 concentration in the building for the JOTAC-OOV-PI, JOTAC-OOV-SS, B-IO-HC, B-IO-PI, B-DO-HC and B-DO-PI, respectively. It may be observed from Fig. 8a that the JOTAC-OOV approach maintains the zonal CO_2 concentration below $O_{\max}$. The drops in the CO_2 concentration values coincide with instances when the AHU damper is maximally opened to introduce air from the ambient to the building for IAQ management. From Figs. 8b and 8c, it may be seen that the instantaneous temperatures in both the lecture halls remain close to 21°C which is the steady state solution for the temperatures in these zones determined by JOTAC-OOV. It is noteworthy, however, that although the underlying optimization framework used for our control strategies aims to minimize total steady state energy consumption, the steady state solutions for zonal temperatures in the hallway remain below $\Delta_3+\delta_3$ for a major part of the day. As the instantaneous zonal temperature tracks these values using either PI control or HC, the central HVAC system supplies the air volume necessary to cool the hallway. The AHU damper position can then be toggled between its extreme positions in lock-step, if the need arises, as described in Section 3.2.2, to ensure that IAQ complies with the prescribed limit at all times. Therefore JOTAC-OOV utilizes the greater temperature flexibility in the hallway to ensure that sufficient air volume, and, by extension, 'fresh' air from the ambient, is supplied to the hallway. These results show that for occupant well-being, both the temperature and ventilation control operations must be jointly determined, rather than the two being agnostic of each other.

Fig. 9a plots the temporal evolution of zonal CO_2 concentration in the building for the JOTAC-FRV-HC approach, whereas Figs. 9b and 9c present the steady state and instantaneous zonal temperatures for the JOTAC-FRV-HC and JOTAC-FRV-PI approaches, respectively. Finally, Figs. 9d and 9e plot the temporal evolution of zonal CO_2 concentration in the building for the JOTAC-FRV-PI and JOTAC-FRV-SS approaches, respectively. Fig. 9a shows that beyond 12 PM, the CO_2 concentration exceeds the prescribed $O_{\max}$ value. In order to understand this phenomenon, it is necessary to recall the stage-wise exposition of JOTAC-FRV from Section 3.2.2. The JOTAC-FRV approach determines the instantaneous AHU damper position based on the zonal temperature and mass flow rates which minimize energy consumption at the steady state. Unlike JOTAC-OOV, ventilation control operations in JOTAC-FRV are determined before the dynamic temperature control operations. The PI/HC dynamic temperature control loop determines the zonal air mass flow rates for tracking the steady state temperature solutions for each zone. Once a zones is

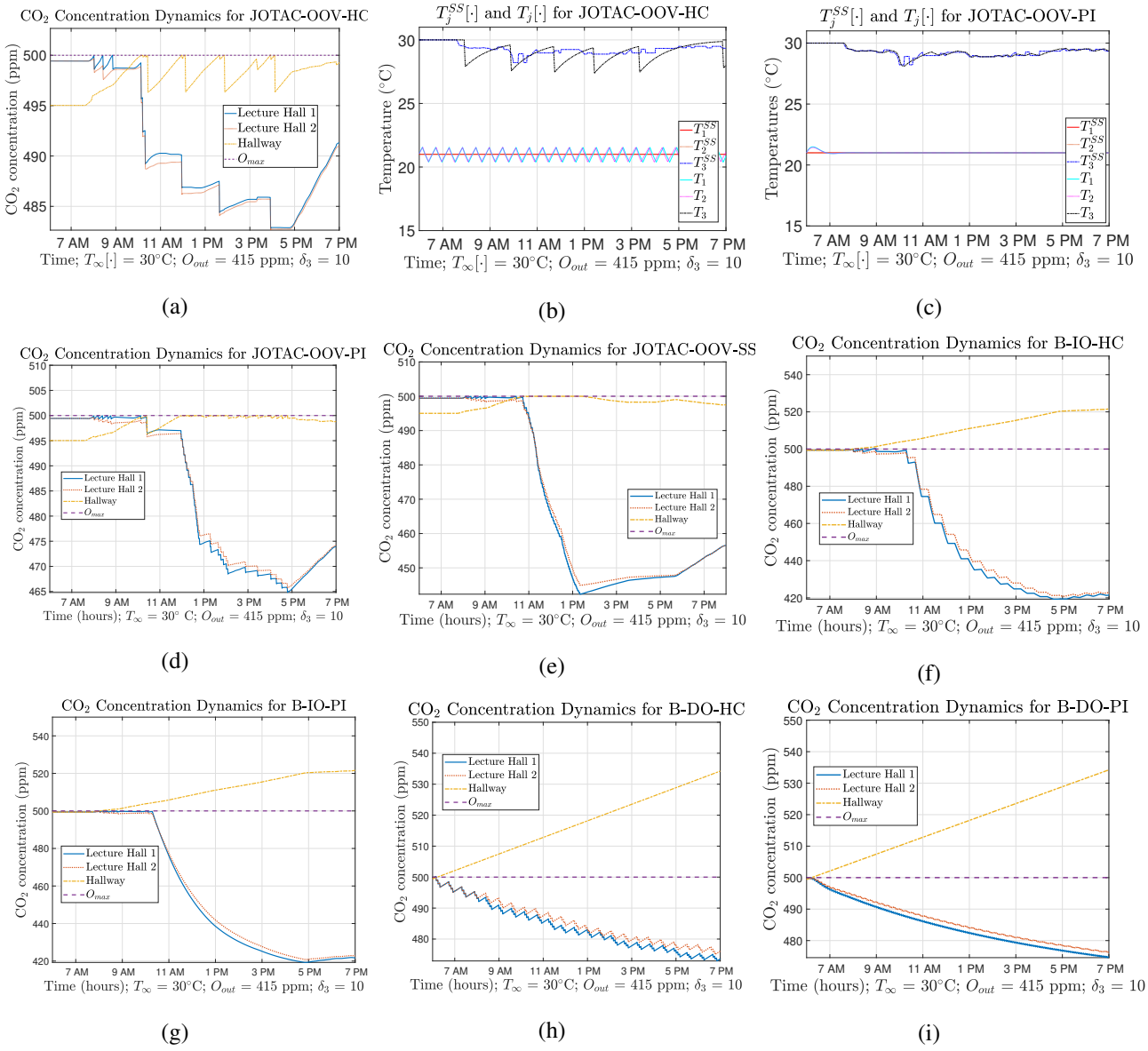

Fig. 8: (a) CO_2 concentration dynamics for JOTAC-OOV-HC, (b) Steady state and instantaneous zonal temperatures for JOTAC-OOV-HC, (c) Steady state and instantaneous zonal temperatures for JOTAC-OOV-PI, for Scenario II under constant ambient temperatures with $O_{\max} = 500$ppm, (d) CO_2 concentration dynamics for JOTAC-OOV-PI, (e) CO_2 concentration dynamics for JOTAC-OOV-SS, (f) CO_2 concentration dynamics for B-IO-HC, (g) CO_2 concentration dynamics for B-IO-PI, (h) CO_2 concentration dynamics for B-DO-HC, (i) CO_2 concentration dynamics for B-DO-PI.

cooled to the desired temperature, the air mass flow rate to that zone is reduced and, in the case of HC, falls to 0. While the zonal mass flow rate is maintained at this low value, the zone may accumulate CO_2 due to a lack of air supply from the ambient. This causes the violation of IAQ standards in the hallway as seen in Fig. 9a. The drops in CO_2 concentration, such as the one recorded at approximately 1 PM can be attributed to the simultaneous decrease in the zonal temperature as evident from Fig. 9b caused by the increased air mass flow rate into that zone.

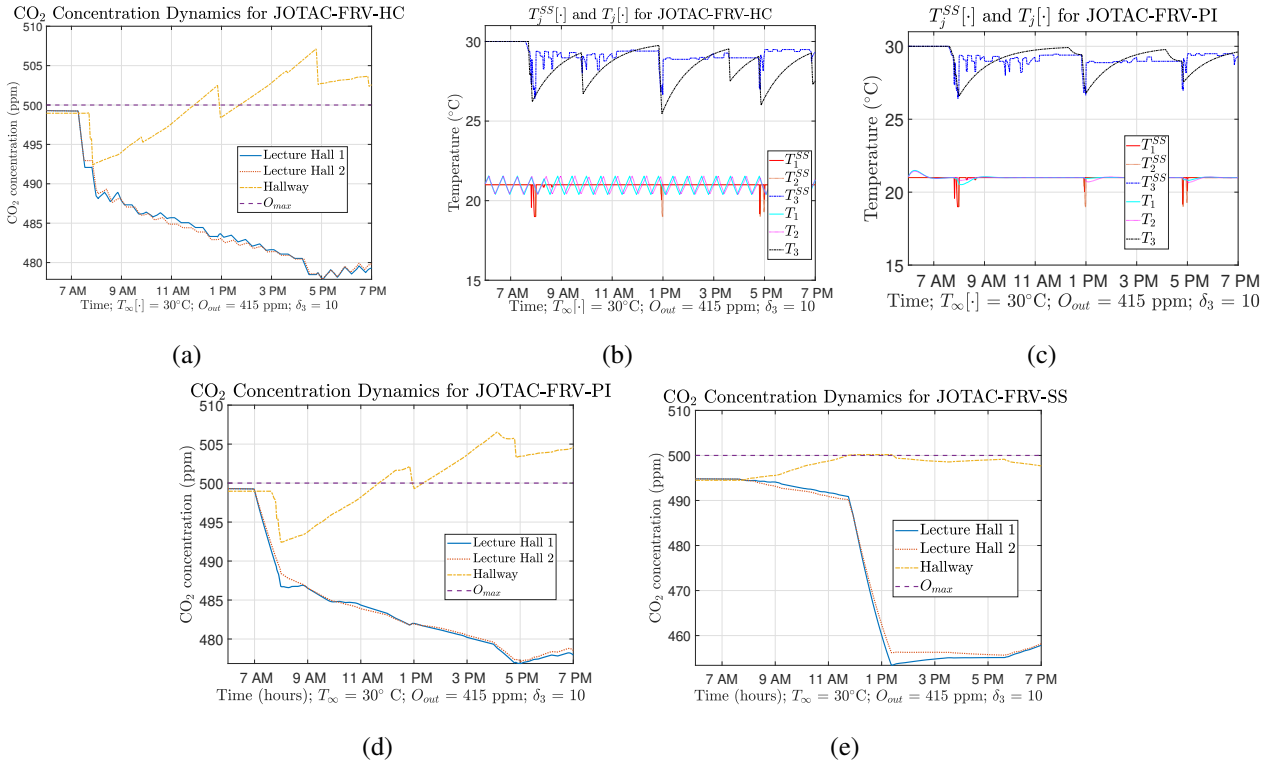

Fig. 9: (a) CO_2 concentration dynamics for JOTAC-FRV-HC, (b) Steady state and instantaneous zonal temperatures for JOTAC-FRV-HC, (c) Steady state and instantaneous zonal temperatures for JOTAC-FRV-PI, for Scenario II under constant ambient temperatures with $O_{\max} = 500$ppm, (d) CO_2 concentration dynamics for JOTAC-FRV-PI, (e) CO_2 concentration dynamics for JOTAC-FRV-SS.

Table III records the energy consumption values for the cooling coil in the VAV HVAC system for our proposed control approaches as well as the baselines for Scenario II under constant ambient temperatures. Furthermore, Table IV records the average violation of the permitted IAQ bounds over the entire 13-hour period for the entire building for each approach. The IAQ violation metric, ζ, is given by, $\zeta = \frac{\sum_{k=1}^{60N}\sum_{j\in\mathcal{J}}\max(O_j[k]-O_{\max},0)}{60N}$, where $N = 13$ hours. It may

be seen from Table III that the JOTAC-OOV-PI, JOTAC-OOV-HC, JOTAC-FRV-PI and JOTAC-FRV-HC approaches consume less power than each of the baselines for each considered value of $O_{\max}$. However, a few comments about the elevated energy consumption values for B-IO-HC and B-IO-PI are in order. As previously noted, these baselines use an on-off ventilation approach similar to the one employed by JOTAC-OOV, while requiring zonal temperatures to necessarily settle at $\Delta_j + \delta_j$, $\forall j$. In the case of the hallway, this means that under the given ambient conditions ($T_\infty[k] = 30°$C, $\forall k$), the zonal mass flow rate of air is zero as $\delta_3 = 10$. This in turn means that air from the ambient cannot be used to improve the IAQ in this zone, thereby causing the IAQ in the hallway to exceed $O_{\max}$. As the temperature and ventilation control operations in the baseline approaches are agnostic of each other, B-IO-HC and B-IO-PI keep the AHU damper maximally open for a prolonged period. With negligible air mass flow into the hallway, this ventilation operation does not help in alleviating the violations in the IAQ in that zone. The entries in Table IV reinforce the aforementioned claims. It may be seen that as the variants of the JOTAC-OOV determined temperature and IAQ management controls jointly, they resulted in minimal violations in IAQ standards. The violations seen for the JOTAC-FRV variants are due to their dependence on steady-state solutions for IAQ management.

TABLE III: Energy consumption of the proposed JOTAC approaches and the baselines (in MJ) for Scenario II with constant ambient temperatures.

$O_{\max}$	**OOV-PI**	**FRV-PI**	**OOV-HC**	**FRV-HC**	**OOV-SS**	**FRV-SS**	**B-DO-HC**	**B-DO-PI**	**B-IO-HC**	**B-IO-PI**
500	29.6	32.9	28.8	33.7	29.4	35.1	34.9	35.1	47.1	47.2
765	29.6	30.3	26.2	30.4	30.6	39.1	34.9	35.1	43.7	44.0
1115	27.5	30.8	26.4	30.6	31.4	29.7	34.9	35.1	40.5	40.3

Another observation that can be made from Table III is that the trends for the energy consumption values for increasing $O_{\max}$ for some variants of the JOTAC approaches are inconclusive, unlike the cases when no or limited ($\delta_j = 1$) zonal temperature flexibility was permitted. This may be attributed to two factors. Firstly, owing to the restricted temperature flexibility in the preceding cases, each zone received sufficient air mass flow which not only maintained zonal temperatures within prescribed bounds but also helped maintain IAQ as zones with lower occupancy helped lower $O_{\text{mix}}[k]$, resulting in the AHU damper being engaged only occasionally. Secondly, as our JOTAC approaches primarily rely on steady state solutions for temperature and IAQ management, the resulting control signals may require some re-evaluations to account for thermal dynamics

TABLE IV: Values of ζ for the proposed JOTAC approaches as well as for the baselines for Scenario II with constant ambient temperatures.

$O_{\max}$	**OOV-PI**	**FRV-PI**	**OOV-HC**	**FRV-HC**	**OOV-SS**	**FRV-SS**	**B-DO-HC**	**B-DO-PI**	**B-IO-HC**	**B-IO-PI**
500	0	1.76	0	1.45	0	0.0213	16.8	16.8	6.69	6.69
765	0	4.02	0	8.07	0	0.227	16.2	16.2	4.87	4.88
1115	0	0.917	0	2.26	0	0	15.5	15.5	2.88	2.88

and ventilation control. The JOTAC-OOV-SS approach is a case in point. Fig. 10 presents the trends for $\bar{\beta}^{*}_{\text{avg}}$, the mean of all values of $\bar{\beta}$ over the course of the 13-hour horizon, $m^{SS*}_{3,\text{ avg}}$, the average mass flow rate of air to the hallway over the same horizon and $\bar{\beta}_{\text{avg}}$, the mean of $\beta[k]$ over the entire horizon. It may be seen that $m^{SS*}_{3,\text{ avg}}$ falls with increasing $O_{\max}$ due to the increasing gradient between the indoor and outdoor CO_2 concentrations, indicating that the steady state solutions for the zonal temperatures also approach $\Delta_3 + \delta_3$. Similarly, $\bar{\beta}^{*}_{\text{avg}}$ increases with increasing $O_{\max}$, as a small amount of air from the ambient can help meet zonal IAQ requirements at the steady state. However, the low steady state mass flow rates at greater values of $O_{\max}$ to the hallway may not be sufficient to meet the IAQ requirements when the zonal CO_2 concentration undergoes transience. Hence, the AHU damper needs to be maximally open for longer periods to draw in the required amount of air from the ambient. This, in turn, results in an increase in energy consumption as seen in Table III.

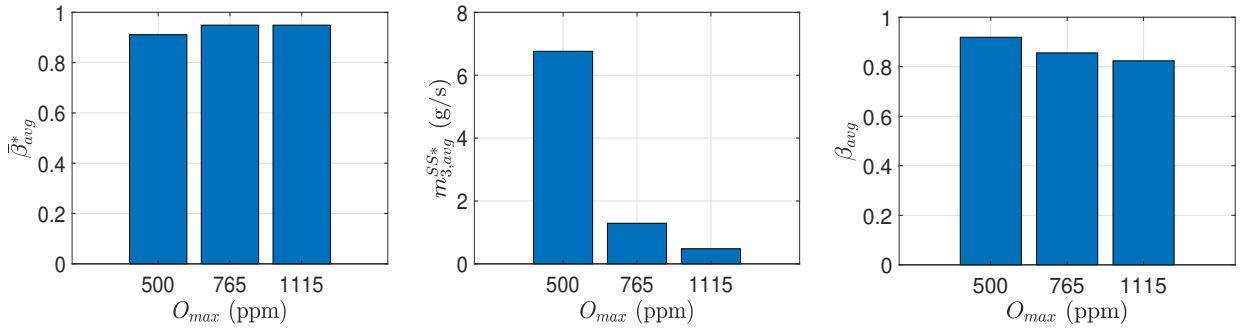

(a) (b) (c)

Fig. 10: Ventilation control and temperature management statistics for the hallway for JOTAC-OOV-SS for Scenario II under constant ambient temperatures.

Fig. 11 shows the % energy savings that may be achieved by permitting zonal temperature

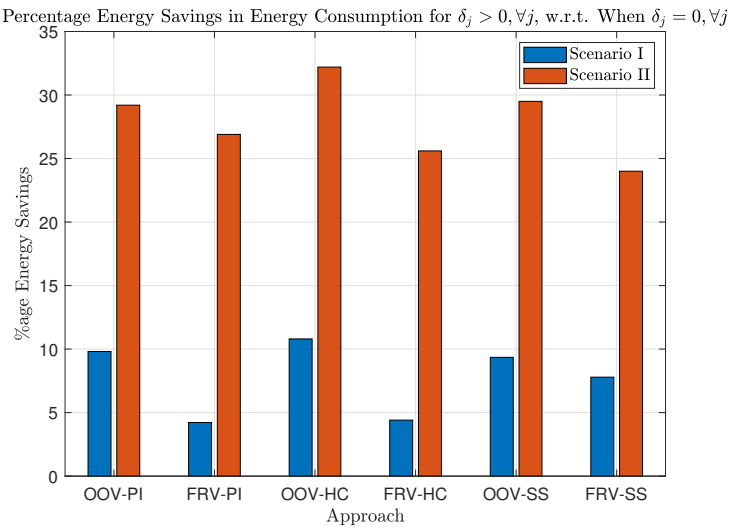

Fig. 11: Percentage (%) savings in energy consumption of the proposed JOTAC approaches when $\delta_j > 0, \forall j$ w.r.t. when $\delta_j = 0, \forall j$, when $O_{\max} = 500$ppm.

flexibility as in Scenarios I and II. It may be seen that the proposed JOTAC approaches can result in energy savings of up to 10.8% under Scenario I as compared to the case where there is no zonal temperature flexibility. Similarly, our proposed approaches were seen to achieve % energy savings of up to 32.2% for Scenario II.

4.4 With Zonal Temperature Flexibility: Scenario II With Changing Ambient Temperatures

We conclude this section by providing numerical results for Scenario II where the ambient temperature changes during the course of the daily building operations for JOTAC-OOV-PI and B-IO-PI. Here, the zonal air mass flow rate is modulated not only due to changing zonal occupancy levels but also due to changing ambient temperatures. In this sub-section, we consider the ambient temperatures witnessed in Albany, NY, for a day in July, 2019, as plotted in Fig. 12 [24]. Due to limited data availability, we assume that the ambient temperatures change linearly during successive hours of the day.

Fig. 13a plots the temporal evolution of the zonal CO_2 concentration for JOTAC-OOV-PI, whereas Figs. 13b and 13c plot the steady state and instantaneous zonal temperatures for JOTAC-OOV-PI and JOTAC-OOV-HC, respectively, for Scenario II with changing ambient temperatures. Figs. 13d and 13e plot the temporal evolution of the zonal CO_2 concentration for JOTAC-OOV-

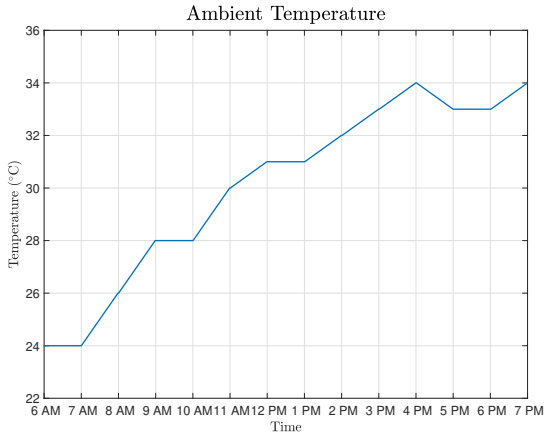

Fig. 12: Changing ambient conditions in Albany on a day in July 2019.

HC and B-IO-PI, respectively. Fig. 13a shows that JOTAC-OOV-PI successfully maintains IAQ within prescribed limits in all zones. Observing Figs. 12, 13a and 13c, it may be seen that between 8 AM and 12 PM, $T_3^{SS}[k]$ remains slightly below $T_\infty[k]$, thereby ensuring that sufficient air mass flow is provided to the hallway to ensure that its IAQ remains within desired limits. As previously mentioned, Scenario II uses $\delta_3 = 10$. Therefore, $T_3^{SS}[k]$ remains at $30°$C beyond 12 PM. For the given gain for the PI-controller, the cooling operation in JOTAC-OOV-PI is significantly damped, with $T_3[k]$ gradually settling at $30°$C. In contrast, the $T_3[k]$ achieves values close to $30°$C much earlier for the JOTAC-OOV-HC approach.

Fig. 14 presents the total energy consumed by JOTAC-OOV-PI and baseline B-IO-PI along with the corresponding values of the IAQ violation metric, ζ. The figure shows that JOTAC-OOV-PI can result in up to approximately 5.4% energy savings as compared to B-IO-PI while ensuring strict adherence to zonal IAQ standards. Furthermore, Fig. 14b shows that, as seen earlier in Table IV, JOTAC-OOV-PI resulted in no CO_2 discomfort being experienced by the building occupants. It may further be noted that while the values of ζ for B-IO-PI are non-trivial for most values of $O_{\max}$ considered here, they are significantly lower than those recorded in Table IV. This observation may be attributed to the fact that the ambient temperatures exceed $30°$C beyond 11 AM. Since, for Scenario II, we take $\delta_3 = 10$ for indoor cooling, the central HVAC system needs to cool the hallway to maintain the indoor temperature close to $30°$C. With sufficient air supply to this zone, baseline B-IO-PI can utilize its ventilation control operations to maintain IAQ within the prescribed limits.

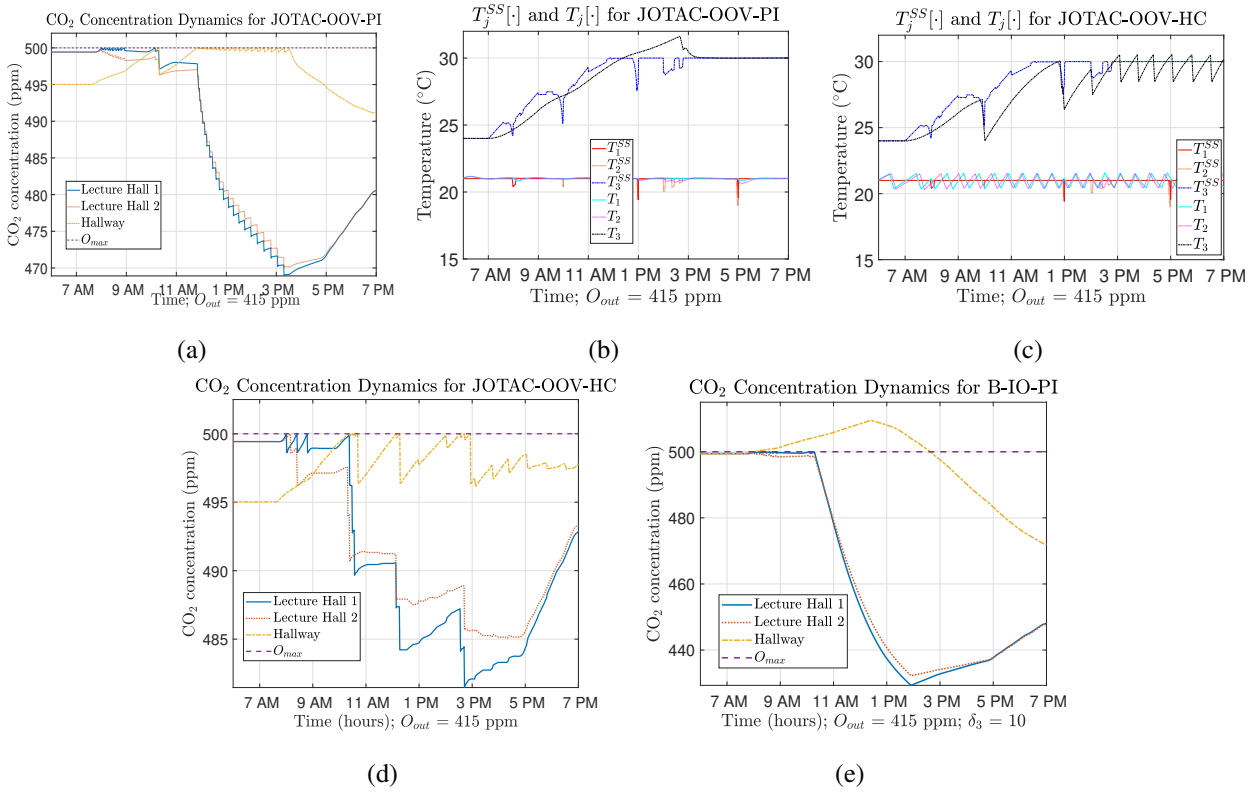

Fig. 13: (a) CO_2 concentration dynamics for JOTAC-OOV-PI, (b) Steady state and instantaneous zonal temperatures for JOTAC-OOV-PI, (c) Steady state and instantaneous zonal temperatures for JOTAC-OOV-HC, (d) CO_2 concentration dynamics for JOTAC-OOV-HC, and (e) CO_2 concentration dynamics for B-IO-PI, for Scenario II for changing ambient temperatures for $O_{\max} = 500$ppm,

5. Conclusion

In this paper, we studied the problem of improving the energy efficiency of a VAV HVAC system in a multi-zone building, while meeting thermal comfort and IAQ requirements. We showed that at steady state, under zonal temperature flexibility, the energy minimization problem for joint thermal and IAQ management is convex when the control variables are taken to be the zonal temperatures. We also showed how the thermal and IAQ management parts of this problem decouple in the absence of zonal temperature flexibility, i.e., when no deviations from given temperature set-points are allowed. Guided by this mathematical analysis, we developed two multi-stage ventilation control mechanisms for reducing the power consumption of the cooling coil of the HVAC system for meeting both the cooling and IAQ requirements of the occupants of

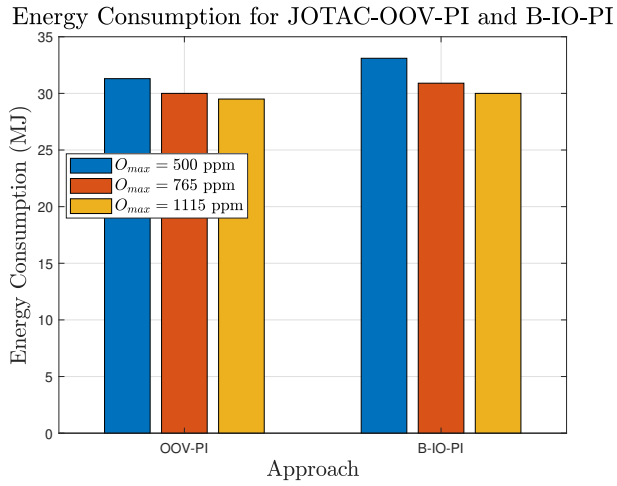

(a)

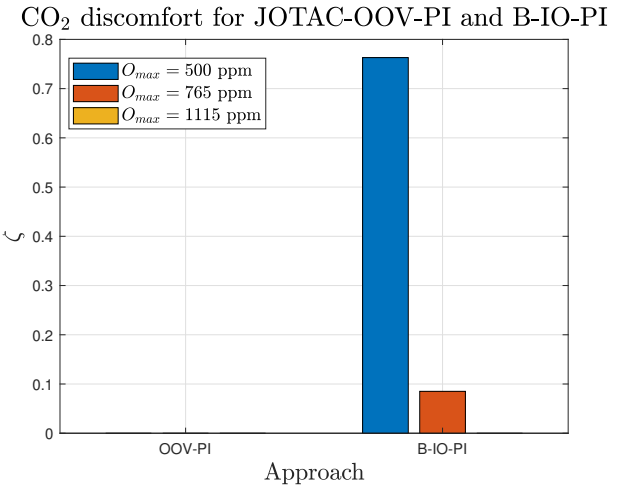

(b)

Fig. 14: Energy consumption and CO_2 discomfort for JOTAC-OOV-PI and B-IO-PI for Scenario II with changing ambient temperatures.

the building. We compared the performance of our proposed approaches with those of multiple baseline approaches which implement separate regimes for controlling zonal temperature and IAQ for a typical work-day in a multi-zone campus building. We evaluated the performance of our proposed approaches under varying levels of flexibility in zonal temperatures. We showed that zonal temperature flexibility can result in energy savings up to 32% (for the same control strategies) as compared to the case where no such flexibility is permitted. Furthermore, our proposed approaches were seen to offer potential savings of nearly 29% compared to the baseline

under certain scenarios. The evaluation of our proposed control strategies using high fidelity building and equipment models, as well as a study into their possible use in managing particulate matter concentration in indoor air, has been left as future work.

6. ACKNOWLEDGEMENT

This work was supported by the National Science Foundation through Award No. 1827546.

REFERENCES

[1] U.S. Department of Energy, "Energy savings potential and RD & D opportunities for commercial building HVAC systems." https://www.energy.gov/sites/prod/files/2017/12/f46/btoDOE-Comm-HVAC-Report-12-21-17.pdf, 2017. [Online; accessed 02-Sep.-2021].

[2] J. Kim, T. Hong, M. Kong, and K. Jeong, "Building occupants' psycho-physiological response to indoor climate and co2 concentration changes in office buildings," *Building and Environment*, vol. 169, p. 106596, 2020.

[3] W. Li, C. Koo, S. H. Cha, T. Hong, and J. Oh, "A novel real-time method for HVAC system operation to improve indoor environmental quality in meeting rooms," *Building and Environment*, vol. 144, pp. 365–385, 2018.

[4] U.S. Department of Energy, "Comfort, indoor air quality, and energy consumption in low energy homes." https://https://www.nrel.gov/docs/fy13osti/56023.pdf, 2013. [Online; accessed 02-Sep.-2021].

[5] Y. Lu, X. Yu, X. Jin, H. Jia, and Y. Mu, "Bi-level optimization framework for buildings to heating grid integration in integrated community energy systems," *IEEE Transactions on Sustainable Energy*, vol. 12, no. 2, pp. 860–873, 2021.

[6] S. K. Gupta, K. Kar, S. Mishra, and J. T. Wen, "Collaborative energy and thermal comfort management through distributed consensus algorithms," *IEEE Transactions on Automation Science and Engineering*, vol. 12, no. 4, pp. 1285–1296, 2015.

[7] S. Taheri and A. Razban, "Learning-based co2 concentration prediction: Application to indoor air quality control using demand-controlled ventilation," *Building and Environment*, vol. 205, p. 108164, 2021.

[8] K. Nam, S. Heo, Q. Li, J. Loy-Benitez, M. Kim, D. Park, and C. Yoo, "A proactive energy-efficient optimal ventilation system using artificial intelligent techniques under outdoor air quality conditions," *Applied Energy*, vol. 266, p. 114893, 2020.

[9] J. Li, J. Wall, and G. Platt, "Indoor air quality control of HVAC system," in *Proceedings of the 2010 International Conference on Modelling, Identification and Control*, pp. 756–761, 2010.

[10] W. Li and S. Wang, "A multi-agent based distributed approach for optimal control of multi-zone ventilation systems considering indoor air quality and energy use," *Applied Energy*, vol. 275, p. 115371, 2020.

[11] Z. Wang and L. Wang, "Intelligent control of ventilation system for energy-efficient buildings with CO_2 predictive model," *IEEE Transactions on Smart Grid*, vol. 4, no. 2, pp. 686–693, 2013.

[12] S. Zhang, Z. Ai, and Z. Lin, "Novel demand-controlled optimization of constant-air-volume mechanical ventilation for indoor air quality, durability and energy saving," *Applied Energy*, vol. 293, p. 116954, 2021.

[13] T. Yang, L. Zhao, W. Li, J. Wu, and A. Y. Zomaya, "Towards healthy and cost-effective indoor environment management in smart homes: A deep reinforcement learning approach," *Applied Energy*, vol. 300, p. 117335, 2021.

[14] W. Valladares, M. Galindo, J. Gutiérrez, W.-C. Wu, K.-K. Liao, J.-C. Liao, K.-C. Lu, and C.-C. Wang, "Energy optimization associated with thermal comfort and indoor air control via a deep reinforcement learning algorithm," *Building and Environment*, vol. 155, pp. 105–117, 2019.

[15] L. Yu, D. Xie, C. Huang, T. Jiang, and Y. Zou, "Energy Optimization of HVAC Systems in Commercial Buildings Considering Indoor Air Quality Management," *IEEE Transactions on Smart Grid*, vol. 10, pp. 5103–5113, Sep. 2019.

[16] Y. Yang, S. Srinivasan, G. Hu, and C. J. Spanos, "Distributed control of multizone hvac systems considering indoor air quality," *IEEE Transactions on Control Systems Technology*, pp. 1–12, 2021.

[17] H. Aglan, "Predictive model for CO2 generation and decay in building envelopes," *Journal of Applied Physics*, vol. 93, pp. 1287–1290, Jan. 2003.

[18] R. Montgomery and R. McDowall, "Chapter 3 - control valves and dampers," in *Fundamentals of HVAC Control Systems* (R. Montgomery and R. McDowall, eds.), pp. 61–105, Oxford: Elsevier, 2008.

[19] NOAA, "Climate change: Atmospheric carbon dioxide." https://www.climate.gov/news-features/understanding-climate/climate-change-atmospheric-carbon-dioxide, 2022. [Online; accessed 20-Sep.-2022].

[20] ANSI/ASHRAE Addendum d to ANSI/ASHRAE Standard 62.1-2016, "Ventilation for acceptable indoor air quality." https://www.ashrae.org/File%20Library/Technical%20Resources/Standards%20and%20Guidelines/Standards%20Addenda/62.1-2016/62_1_2016_d_20180302.pdf, 2016. [Online; accessed 20-Sep.-2022].

[21] ANSI/ASHRAE Addendum s to ANSI/ASHRAE Standard 62.1-2016, "Ventilation for acceptable indoor air quality." https://www.ashrae.org/File%20Library/Technical%20Resources/Standards%20and%20Guidelines/Standards%20Addenda/62.1-2016/62_1_2016_s_20190726.pdf, 2016. [Online; accessed 20-Sep.-2022].

[22] Kwansei Gakuin University, "The area and size of lecture halls and seminar rooms in each undergraduate and graduate school." https://global.kwansei.ac.jp/cms/kwansei_foreign/pdf/about/facts/basicdata/2012/0000051081.pdf, 2012. [Online; accessed 20-Sep.-2022].

[23] M. Sherman, "Efficacy of intermittent ventilation for providing acceptable indoor air quality." https://www.osti.gov/servlets/purl/834643-ervtNw/native/. [Online; accessed 20-Sep.-2022].

[24] "Weather in July 2019 in Albany, New York, USA." https://www.timeanddate.com/weather/usa/albany-ny/historic?month=7&year=2019. [Online; accessed 20-Sep.-2022].